A biochemical framework for modeling the functional metabolism of the human brain

Mauro Di Nuzzo[1], Federico Giove[1,2], Bruno Maraviglia[1,3]

1. Dipartimento di Fisica, Sapienza Università di Roma, Rome, Italy

2. MARBILab, Museo storico della fisica e Centro di studi e ricerche "Enrico Fermi" Rome, Italy

3. Fondazione Santa Lucia IRCCS, Rome, Italy.

The existence of complex control mechanisms in the catabolism of molecules utilized for energy production forms the basis of the relationship between function and metabolic regulation. This is especially important in the brain, where numerous *in vitro* and *in vivo* experiments have lend support to the theory of the coupling between neuronal activity and energy metabolism, a view enlightened several decades ago and now consolidated. Notwithstanding, many details remained unresolved about the fate of nutrients within the brain parenchyma and the consequent exchanges of substances, particularly between neurons and astrocytes, whose involvement in the neurometabolic coupling is well established. Unfortunately, due to limited spatial and temporal resolution, the currently available experimental techniques do not allow specific measurements of cerebral metabolites in different cell types *in situ*. Therefore, the analysis of the incomplete experimental data requires the formulation and application of mathematical models. In this paper, we explore these theoretical accounts in the construction of a unified biochemical framework of supply and demand in the context of compartmentalized brain energy metabolism. The model successfully predicts the time-course of observable variables, while providing information about a number of processes underlying neural activity. Future work is expected to gain insights by testing the model with respect to different hypotheses about transport and metabolic cell specialization, as well as about the degree of activation of neurons and astrocytes following brain stimulation.

Abbreviations used: ADC, apparent diffusion coefficient; ADP, adenosine 5'-diphosphate; AK, adenylate kinase; AMP, adenosine 5'-monophosphate; ANLS, astrocyte-neuron lactate shuttle; ATP, adenosine 5'-triphosphate; BBB, blood-brain barrier; CBF, cerebral blood flow; CK, creatine kinase; CMRGlc, cerebral metabolic rate of glucose; $CMRO_2$, cerebral metabolic rate of oxygen; Cr, creatine; ECM, extracellular matrix; fMRI, functional magnetic resonance imaging; GAP, glyceraldehyde-phosphate; GLUT, glucose transporter; HK, hexokinase; LAC, lactate; LDH, lactate dehydrogenase; MCT, monocarboxylate transporter; NADH, nicotinamide adenine dinucleotide; OGI, oxygen-glucose index; PCr, phosphocreatine; PDH, pyruvate dehydrogenase; PEP, phosphoenolpyruvate; PET, positron emission tomography; PFK, phosphofructokinase; PGK, phosphoglycerate kinase; PK, pyruvate kinase; PYR, pyruvate; TCA, tricarboxylic acid cycle.

Address correspondence to Mauro DiNuzzo, Magnetic Resonance for Brain Investigation Laboratory, Fondazione Santa Lucia IRCCS, Via Ardeatina 306, 00179 Roma, Italy. E-mail: mauro.dinuzzo@roma1.infn.it

1 Introduction

The brain possesses several intrinsic mechanisms that couple neural activity to the vascular response, which are activated by a number of metabolic products whose relevant pathways are up- or down-regulated. The understanding of this functional metabolic response has been made difficult by the recent concern of astroglial cells in many aspects of brain physiology. Astrocytes have been historically recognized as sole supportive cells, yet they have a primary role in chemical neurotransmission and vascular regulation [1]. In fact, on the one hand astrocytes are in close proximity to the synaptic element, and on the other they participate to the formation of the blood-brain barrier (BBB), thereby contributing to mediate the access of nutrients to the brain parenchyma. The involvement of astrocytes in the coupling between neuronal activity and metabolism is awarded by the potential for these cells to respond to synaptic activity with intracellular metabolic cascades which have effects of both vasodilation and vasoconstriction on smooth muscle cells surrounding cerebral arterioles [2]. Moreover, the emergence of novel astrocytic functions entailed a crescent role of astrocytes in neurometabolic coupling, classically exclusive of neurons. Indeed, the central dogma of brain metabolism tied neuronal activity alone to the cerebral metabolic rate of glucose and oxygen [3, 4]. On the opposite, in brain regions of focal activation an increase of anaerobic metabolism and a concomitant accumulation of lactate is observed [5, 6]. Further, the finding that the principal excitatory neurotransmitter of the central nervous system L-glutamate stimulates the release of lactate by cultured astrocytes [7] led to the hypothesis that neurons may utilize considerable lactate derived by astrocytes in intact tissue. More importantly, according to this view astrocytes would represent the primary site of brain glucose uptake. In spite of its formal coherence, the plausibility of such a scenario, which is known as the astrocyte to neuron lactate shuttle (ANLS), remains widely debated. In fact, no conclusive proofs have been produced that neurons utilize preferentially astrocyte-derived lactate during their physiological activity [8, 9].

The fallacy in performing conclusive measurements about glucose and lactate fluxes within the brain favored the recent appearance of modeling perspectives dealing with functional cerebral metabolism. Nonetheless, complications arise due to the heterogeneous character of the tissue emerging from the complex ultrastructural features as well as from the enzymatic specialization of individual cell types. Both aspects lift the metabolic network in order to ensure the maintenance of far-from-equilibrium metabolites homeostasis and its adaptation to a varying demand, thereby providing a link between function and metabolic regulation. It is interesting to investigate how this shapes the metabolic network in the brain, which is known to possess a highly compartmentalized metabolism and where the trafficking of substances between different cell types is thought to be central. Recently, several mathematical models have appeared that describe the physiological processes which characterize the functional activation of neural cells in relation to brain metabolism [10–12]. Since theoretical models use several *a priori* assumptions to obtain reliable results, it is advisable to limit the number of required premises by combining all the available theoretical information of nutrients transport and catabolism in the brain tissue. Here, we unified the current quantitative description of metabolic and physiological cellular processes with the detailed kinetic properties of substance delivery to the brain. Noticeably, we obtained results in agreement with the classical view of the cerebral metabolism, with glucose primarily taken up by neurons. Furthermore, simulations showed that the neuronal element likely represents the cellular origin of excess lactate produced following brain activation. After its validation process [11, 12], metabolic modeling of the human brain can be capitalized as a tool to test hypotheses and guide experi-

mental strategies. Moreover, comprehending the metabolic details underlying brain activity is fundamental inasmuch as the functional images of activated brain areas obtained with functional magnetic resonance imaging (fMRI) or positron emission tomography (PET) are produced by the signal created by the cerebral metabolism. Thus, results of mathematical models may help in understanding how imaging methods relate to the activity of the resting and stimulated brain.

2   Methods—Description of the model

The mathematical description of cell metabolism can be implemented essentially according to two different representations, which rest on the stoichiometric [13] or the kinetic modeling approach [14]. The former assumes the existence of a pseudo steady-state for metabolic intermediates, thereby warranting flux analysis based basically on mass balance (reviewed by [15]). However, because of the inherently dynamic nature of all metabolic processes, this method places severe limitation which are difficult to get around without imposing additional constraints [16]. On the other hand, kinetic modeling is made complicated by the requirement of individual reaction rate equations containing a large number of parameters which, especially for large scale metabolic networks, have to face the scarcity of experimental data. To date no reliable stoichiometric approaches exist to take into account the feedback that transient changes in metabolite concentrations exert on the time-dependent regulatory mechanisms of the cell metabolism, although several attempts appear to be promising (see [17]). The dynamic metabolic status that distinguishes each separate instant within the overall time-course of metabolic intermediates is far from being compatible with a steadiness condition. Therefore, since our primary interest is to appreciate the metabolic response to altered physiologic activity, we conformed to the kinetic modeling strategy embracing some established mathematical descriptions of enzyme-catalyzed reactions and transport processes.

The mathematical equations illustrated here for the various aspects of the cerebral physiology have been integrated into a consistent and unified biochemical framework. It is worth noting that the physiological mechanisms coupling the brain electrical signaling with metabolism and hemodynamics are independently regulated, although the cerebral circulation is promptly adjusted to meet the metabolic demand of the tissue [18]. In particular, metabolic activity is primarily dictated by the energy demand of Na^+/K^+–ATPase, whereas hemodynamic response grounds on several molecular cues only indirectly related to the work of the pump [2]. Therefore, the description of these processes has to be earned through experimental evidence, when available, or theoretical calculations. A detailed description of the qualitative and quantitative information which guided the theoretical strategies employed in the present modeling work can be found in the appendix.

We adopted the convention that outward fluxes are positive and inward fluxes are negative, where transport rates are expressed for unit of destination cellular compartment. For example, glucose flux j_{GLC}^{in} from interstitium to neuron is expressed for unit neuronal volume. Thus, balance equation for neuronal glucose is written as

$$V_n \frac{d}{dt}[GLC_n] = V_n j_{GLC}^{in} - V_n v_{HKPFK}^n \qquad (1)$$

where the neuronal volume fraction V_n can be canceled out. In order to adapt transport equations with different units of parameter values, expressed either for unit cellular compartment [11] or absolute activity [12], the relevant flux has to be divided for the absolute compartment volume which is interested in the process. For

example, the equation for $j_{\text{GLC}}^{\text{in}}$ (units mmol/L/s) changes to

$$j_{\text{GLC}}^{\text{in}} = \frac{1}{U_{\text{n}}} J_{\text{GLC}}^{\text{in}} \tag{2}$$

where U_{n} is the absolute neuronal volume (units L) and $J_{\text{GLC}}^{\text{in}}$ the absolute glucose flux (units mmol/s). Turning now to the interstitial glucose balance equation, according to our convention it is written as

$$\frac{d}{dt}[\text{GLC}_{\text{i}}] = j_{\text{GLC}}^{\text{bi}} - \left(\frac{V_{\text{n}}}{V_{\text{i}}}\right) j_{\text{GLC}}^{\text{in}} - j_{\text{GLC}}^{\text{gi}} \tag{3}$$

whereas the same equation in terms of absolute fluxes is given by

$$\frac{d}{dt}[\text{GLC}_{\text{i}}] = \frac{1}{U_{\text{i}}} \left[J_{\text{GLC}}^{\text{bi}} - J_{\text{GLC}}^{\text{in}} - J_{\text{GLC}}^{\text{gi}} \right] \tag{4}$$

where U_{i} is the absolute interstitial volume. Accordingly, the following relations can be stated

$$j_{\text{GLC}}^{\text{bi}} = \frac{1}{U_{\text{i}}} J_{\text{GLC}}^{\text{bi}} \tag{5}$$

$$j_{\text{GLC}}^{\text{in}} = \frac{1}{U_{\text{i}}} \left(\frac{V_{\text{i}}}{V_{\text{n}}}\right) J_{\text{GLC}}^{\text{in}} \tag{6}$$

$$j_{\text{GLC}}^{\text{gi}} = \frac{1}{U_{\text{i}}} J_{\text{GLC}}^{\text{gi}} \tag{7}$$

We used the procedure sketched above to calculate all other fluxes, thereby obtaining a homogeneous system of ODEs.

It is straightforward that equations (2) and (6) can not be met simultaneously unless the ratio of absolute volumes matches the corresponding fractional ratio. Unfortunately, the pertinent mathematical descriptions [11, 12] considered slightly different cellular volume fractions, resulting in a few percent difference in maximum transport rates. Howsoever, careful analysis of minor changes to transport velocities confirmed that both the qualitative and quantitative response of the model is almost unaffected, whilst the effect of substantial alterations of transport rates has been systematically examined elsewhere [12].

In addition, adjustment of reaction rates was carried out in order to adapt the transport of substances to their catabolism when assessing the impact of different neuronal vs astrocytic glycolytic or oxidative ratios. For example, in order to modify the cell oxidative capacity we recast the equation for tissue mitochondrial respiration rate

$$v_{\text{Mito}}^{\text{tissue}} = V_{\text{n}} v_{\text{Mito}}^{\text{n}} + V_{\text{g}} v_{\text{Mito}}^{\text{g}} \tag{8}$$

as

$$\beta v_{\text{Mito}}^{\text{tissue}} = \alpha_{\text{n}} V_{\text{n}} v_{\text{Mito}}^{\text{n}} + \alpha_{\text{g}} V_{\text{g}} v_{\text{Mito}}^{\text{g}} \tag{9}$$

where α_{n} and α_{g} are multiplicative factors for neuronal and astrocytic mitochondrial rate, respectively, which are necessary to obtain the fraction β of the original overall rate. Considering the original oxidative ratio r defined as

$$r = \frac{v_{\text{Mito}}^{\text{n}}}{v_{\text{Mito}}^{\text{g}}} \tag{10}$$

and the desired ratio R given by

$$R = \frac{\alpha_{\text{n}} v_{\text{Mito}}^{\text{n}}}{\alpha_{\text{g}} v_{\text{Mito}}^{\text{g}}} = \frac{\alpha_{\text{n}}}{\alpha_{\text{g}}} r \tag{11}$$

the unknown constants α_n and α_g can be calculated as

$$\alpha_n = \frac{\beta r}{R} \left[\frac{1 + r(V_n/V_g)}{1 + R(V_n/V_g)} \right] \tag{12}$$

$$\alpha_g = \beta \left[\frac{1 + r(V_n/V_g)}{1 + R(V_n/V_g)} \right] \tag{13}$$

Following this operation, minor adjustment were necessary in order to maintain intracellular metabolites concentrations as close as possible to the original steady-state levels, while leaving tissue oxidative metabolism unaltered ($\beta = 1$) or slightly modified ($\beta \neq 1$). In particular, oxygen diffusion rates j_{O2}^{cn} and j_{O2}^{cg}, and ATPases activities $v_{ATPases}^n$ and $v_{ATPases}^g$ have to be multiplied by the corresponding α constant. Eventually, small changes have to be applied to hexokinase-phosphofructokinase system rates k_{HKPFK}^n and k_{HKPFK}^g to attune basal CMRGlc and CMRO$_2$.

The simulations were carried out by Rosenbrock numerical integration for stiff problems using the software package MATLAB version 7.0.4 R14 (The MathWorks Inc., Natick, MA, USA). In particular, the algorithm allows the solution of the initial value problem

$$y' = F(t, y) \tag{14}$$

on the time interval $[t_0, t_f]$, given initial values $y(t_0) = y_0$. It is based on numerical differentiation formulas (NDFs) with changing step-size. Specifically, the solver forms a new Jacobian of the system at every step and monitors the convergence of the solutions, whereby increasing or reducing the step size accordingly (see the MATLAB user manual for detailed references).

3   Results and discussion

A wealth of cerebral biochemical and biophysical processes are heterogeneously regulated at the cellular and subcellular level according to a specific correspondence with the physiologic activity of the brain. Unfortunately, the modalities of this correspondence have been not yet completely understood, thus lingering the question about exactly how the events experienced by a regional ensemble of neurons and astrocytes can be fastened together in the concept of brain activation. Cerebral cells react to dramatic, energy-consuming processes taking place in the milliseconds timescale range, whose effect is represented by a number of alterations in the cellular environment important enough to rationalize the definition of a particular state of these cells called activation. This condition brings about a definite metabolic response covering the energetic replenishment of brain cells, which is currently well characterized only at the organ level. Nevertheless, comprehending the brain metabolism at the cellular level is advisable inasmuch as the cerebral machinery grounds in an elaborate collaboration between different cell types whose subcellular constituents are extremely intermingled [19].

Due to the exceptionally high metabolic rate of the brain, the lack of oxygen and glucose in the tissue as a result of compromised blood supply is especially detrimental for cerebral cells—i.e. neurons and astrocytes. This exceptional cellular sensitivity to nutrients deprivation is ideally evidenced by the onset of unconsciousness within about 10 seconds after blood flow blockage. In fact, the large metabolic demand of neural activity and the relative stability of the overall brain energy consumption pose a severe limitation in energy allocation, which constrain the brain to a high degree of flexibility in distributing the fraction of cells working at any time [20]. This reorganization produces a concomitant focal alteration in the regional tissue energy
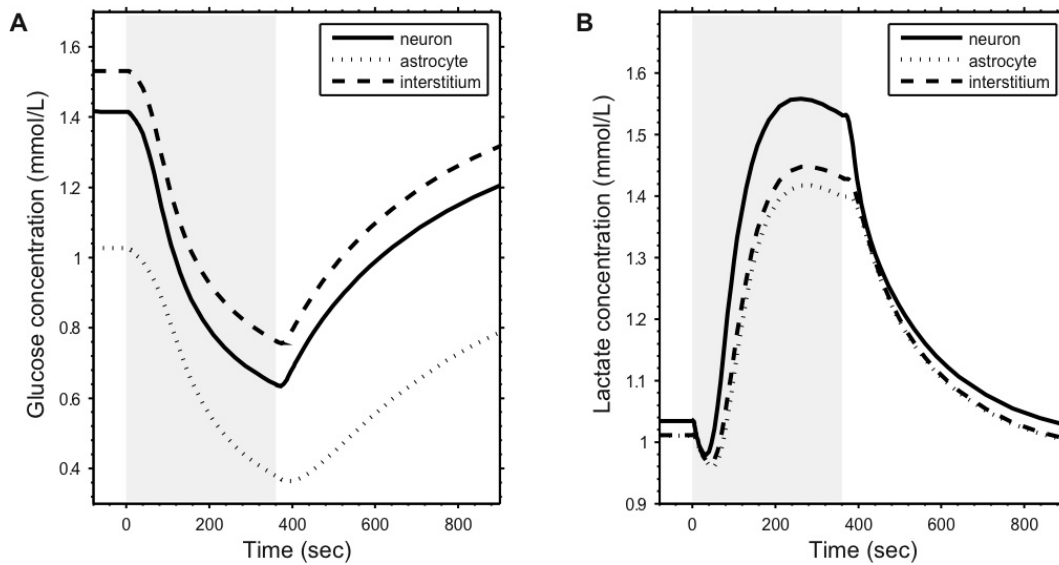
Figure 1: Model results for (**A**) glucose and (**B**) lactate concentration transients. Both simulated metabolite time-courses are in qualitative and quantitative agreement with experimental data. Specifically, glucose reaches a minimum at the end of stimulation interval, whereas, after an initial dip, lactate increases after the stimulation onset and then start decreasing prior to the end of stimulation (see text for details).

requirement which affects the dispensation of metabolic substrates to and between operative cells within multiple functional and structural restraints. Unfortunately, the elucidation of the relationship between the resulting metabolic reaction and the extent of cellular stress needed to observe it, which may be more or less physiological, is far from definite. However, the elusive character of the latter point can be exceeded by recasting neuronal activation to a local and acute phenomenon which require a sustained brain stimulation for seconds or even minutes. Therefore, we tested the model following a 360-sec activation, which is a time period in the range of those commonly used in visual stimulation paradigms. Furthermore, a direct comparison with results obtained by Frahm and colleagues [21, 22] is possible by making the choice of 6 minutes stimulation.

Simulation of basal brain metabolites levels were consistent with experimental data [11, 12]. Besides steady-state metabolites concentrations, the model allows to evaluate the dynamics of the relevant metabolites during brain activation. In particular, tissue glucose transient reduction resulting from simulations (Figure 1A) is consistent with experimental data which reported glucose decreases in the range 10% to 60% [21–32]. The model also succesfully reproduced the increase of lactate concentration (Figure 1B) observed during brain activation, which reported lactate rise in the range 20% to 180% [6, 21, 22, 29, 33–42]. It should be realized that the actual dynamics of glucose and lactate concentration may vary according to the type of stimulation. For example, the observed lactate concentration peak is smaller and delayed for cognitive activations with respect to visual, auditory or motor stimulations. The model can provide adequate results for several metabolite time courses, namely glyceraldehyde 3-phosphate (GAP) (Figure 2A), phosphoenolpyruvate (PEP) (Figure 2B) and intracellular oxygen (Figure 2C) [5, 43, 44]. The theoretical data is compatible with the experimental findings, which suggest a switch to anaerobic metabolism in
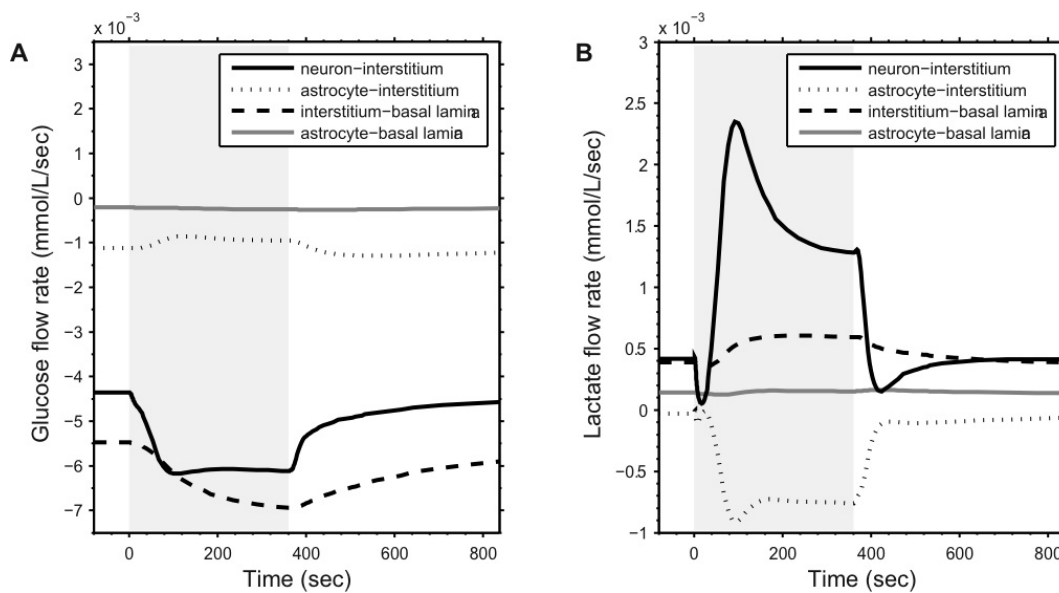
Figure 2: Simulated time-course of some metabolic intermediates. (**A**) Glyceraldehyde 3-phosphate (GAP), (**B**) Phosphoenolpyruvate (PEP), (**C**) Oxygen (O_2), (**D**) Nicotinamide adenine dinucleotide (NADH), (**E**) Phosphocreatine (PCr), and (**F**) Adenosine triphosphate (ATP). Simulated concentration transients reflect experimentally measured changes. In particular, the glycolytic intermediates and phosphocreatine drop to a minimum during the stimulation. NADH displays a biphasic time-course which reflects lactate dynamics (see Figure 1). Note that ATP homeostasis favors phosphocreatine depletion and lactate accumulation over pyruvate oxidation in the early phase of the stimulation. In the late phase of the stimulation, lactate (after conversion to pyruvate by LDH) is consumed by mitochondrial respiration.

the early phase of neuronal activation, followed by a reversion to aerobic metabolism in the late phase. In particular, glucose consumption, as evidenced by the decrease in glucose concentration, lasts even after the lactate accumulation and clearance (Figure 1A,B).

Notably, the model proved to be also capable of reproducing the brief lactate initial dip ($\sim 10\%$) following stimulation onset (Figure 1B) [8]. The simulated evolution of extracellular lactate, which displays a small initial dip followed by a larger increase, is consistent with experimental extracellular lactate monitoring in rats [45]. The biphasic dynamics of lactate is reflected in a similar time-course of the tissue (both neuronal and astrocytic) $NADH/NAD^+$ ratio as reflected by NADH concentration (Figure 2D), which shows a large increase during enhanced glycolysis with a preceding decrease due to ADP-mediated stimulation of oxidative phosphorylation, in agreement with experimental findings [46–48]. However, the origin (cytoplasmic versus mitochondrial, and neuronal versus astrocytic) of the NADH signal is subjected to debate [11], and the model is unable to highlight any significant specific monophasic response in neurons or astrocytes. Energy consumption gives rise to a considerable decrease in phosphocreatine (PCr) concentration (Figure 2E), while ATP is maintained at a relatively stable level (Figure 2F), thus preserving cellular energy homeostasis [49]. Accordingly, ATP and PCr time courses produced by the model fit qualitatively with experimental data obtained with ^{31}P MRS during stimulation of human primary visual cortex [38], that show a sharp decrease in $[PCr]/[P_i]$ ratio and a moderate concomitant decrease in the ratio $[ATP]/[P_i]$.
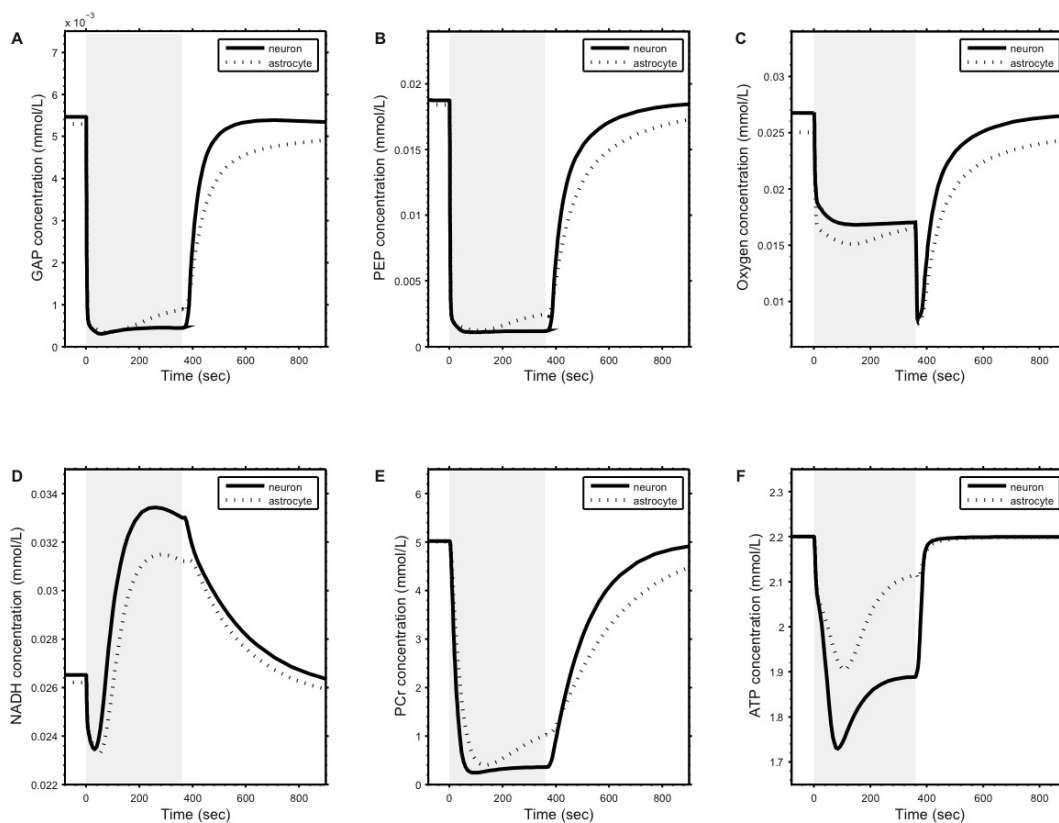
Figure 3: Theoretical model outcomes for (**A**) glucose and (**B**) lactate fluxes. Blood-borne glucose is primarily taken up by neurons through basal lamina in resting conditions. Upon stimulation, the sugar is channeled to neurons first via high-capacity neuronal GLUTs. Concomitant glucose uptake by astrocytes is reduced during stimulation, whereby astrocytes use neuron-derived lactate. Note however that, in terms of carbon equivalents, the intercellularly shuttled lactate during stimulation represents only a few percent of the glucose taken up by the brain in the same interval. The amount of lactate transferred between neurons and astrocytes is comparable to the concurrent washout of the monocarboxylate by the bloodstream (via basal lamina).

Simulations showed that glucose is primarily taken up by neurons, at rest (~ 5 times more than astrocytes) and even more under stimulation, when astrocytic glucose uptake decreases (Figure 3A). Concomitantly, activation-induced lactate trafficking accounts for the flow of the monocarboxylate from neurons to astrocytes (Figure 3B). The stimulation-derived increase in extracellular lactate is required in order to keep intracellular lactate levels low enough to enable neuronal and astrocytic aerobic glycolysis to continue [3, 50]. However, if elevated extracellular lactate happens to re-enter cells, it is more likely to enter astrocytes than neurons because of the kinetic properties of neuronal monocarboxylate transporter MCT2, which is 60% saturated at the resting lactate level [51]. This is indeed the result of the simulations, where during neuronal activation the larger energy demand is accounted for by neurons, which is in agreement with recent findings obtained in cellular cultures. In particular, in these experiments neurons appeared to utilize lactate more extensively than glucose to maintain metabolism only under resting conditions, while glucose resumed as the preferred substrate during synaptic activity [52–54]. Moreover, it has been found that cultured astrocytes oxidized lactate at 3 times the rate of glucose [55]. Cultured
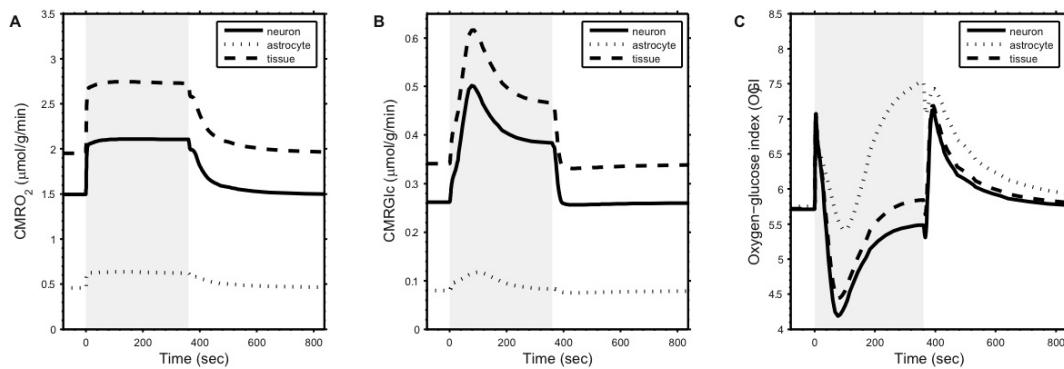
Figure 4: Simulations of cerebral metabolic rate of (**A**) oxygen (CMRO$_2$) and (**B**) glucose (CMRGlc). (**C**) Time-course of oxygen/glucose index (OGI). The major contribution to the uncoupling between glucose and oxygen utilization during stimulation is accounted for by neurons. Under this specific simulated condition, the glucose taken up by astrocytes is almost completely oxidized, while the astrocytic OGI higher than 6 represents the oxidation of neuron-derived lactate.

glia also failed to maintain normal ion gradients when their oxidative metabolism was inhibited with rotenone, while glycolysis was still being maintained with glucose [56]. The results that we obtained from the developed model are consistent with a dependence of lactate transients evolution on neuronal energy demand during activation, and with an astrocytic lactate uptake under such circumstances [12].

The question is not whether neurons normally use astrocyte-derived lactate, but rather which are the lactate fluxes during physiological neural activation *in vivo*, and this question has not yet been answered experimentally. Physiological stimulation has been observed to increase brain lactate concentration (see [57]), and glycogenolysis as well [58]. From the magnitude and the rate of these increases, it can be inferred that neuronal activation had led to an increase in glycolysis. Although this increase is out of proportion to any increase of oxidative metabolism, it should be noted that oxidative phosphorylation also increases in response to physiological activity [5,59–63]. Furthermore, oxidative metabolism is much more efficient than glycolysis, so that most of the additional energy required for activity is still provided by oxidative metabolism (see [64]). It remains to be assessed whether the rise of glycolysis can be explained by a Pasteur effect due to oxygen limitations, or to a shift in the nature of the energy demands toward reactions that are normally served by glycolysis [65]. It should be realized, however, that the observed increase in tissue lactate concentration following brain stimulation can represent a process of the normal physiology of the brain, rather than a mere increase of anaerobic glycolysis. Accordingly, it has been put forward that lactate may be the major product of glycolysis, whether aerobic or anaerobic, and thus the principal substrate for the mitochondrial tricarboxylic acid cycle [66].

It is possible to examine the time-course of oxygen/glucose index (OGI), which equals CMRO$_2$/CMRGlc—i.e. the ratio between cerebral metabolic rate of oxygen and glucose, respectively. During activation, the increase in CMRO$_2$ (Figure 4A) is accompanied to a even larger activation-dependent stimulation of CMRGlc (Figure 4B) [67]. Accordingly, OGI (Figure 4C) falls from its resting value (~ 5.5 to ~ 4) reflecting nonoxidative metabolism of glucose, which is in agreement with experimental data showing values between 4 and 5 during activation (see [68] and references

therein). OGI values greater than the theoretical value of 6 at the beginning of the stimulation and in the post-stimulus period are accounted for by neuronal bursts of oxidative metabolism. Indeed, the experimental time course of the cerebral blood oxygenation displays an initial hyper-oxygenation due to elevated blood flow (with an unchanged oxygen utilization) followed by an hypo-oxygenation caused by a decreased blood flow during a still active aerobic metabolism, indicating a shift in the brain metabolism from anaerobic to aerobic in the course of activation [21]. In other words, the observed uncoupling between $CMRO_2$ and CMRGlc is reduced to the early period of brain stimulation.

Perhaps, the most striking result that we earned with the present model is the support for the central dogma of cerebral energy metabolism, endorsing the view that glucose is the major energetic fuel of neuronal activity [3]. Furthermore, the model uphold another traditional assumption of brain metabolism, which states that the majority of cerebral glucose utilization sustain neuronal activity via oxidative metabolism, both at rest and during activation [4]. The present modeling results sharply contrast with those derived in [11], whilst they are in good agreement with the theoretical outcomes obtained in [12]. Notably, the set of parameters and the rate equations are the same of original models, except for those values that are not supported by current literature. Specifically, to the description of Aubert and Costalat [11] we added the novel detailed model of nutrient transport across the blooodbrain barrier and within the brain parenchyma [12] as well as the recent experimental data about metabolic self-sufficiency of neurons and astrocytes [69,70]. The inclusion of these theoretical and experimental data proved sufficient to change the results of the original models. We also performed local sensitivity analysis on all parameter values as the time-derivative of all reaction/transport rate equations with respect to every model parameter. This showed largely distributed impact of parameters on model outcomes, thereby indicating the robustness of the mathematical description. Furthermore, the results of the model have been tested under several sets of assumptions related to the metabolic capacity of individual cell types, glucose and lactate transport competence, and degree of stimulation of neurons and astrocytes (see [71] for details).

The primacy of neuronal glucose oxidation established the classical view of cerebral energy metabolism, which is presently withstood by many researchers [9,72,73]. The model outcomes theoretically confirm these facets by providing a major neuronal contribution to CMRGlc and $CMRO_2$. Resting glucose and oxygen cerebral metabolic rates (Figure 4A,B) quantitatively follow the experimental estimates ranging from 0.28 to 0.43 μmol/g/min for CMRGlc and from 1.39 to 1.90 μmol/g/min for $CMRO_2$ [74–78]. A significant increase in CMRGlc during neuronal stimulation (Figure 4B) in the range 12-50% was reported by many authors using several experimental methods [5,21–23,32,79,80], whereas a more modest increase in $CMRO_2$ (Figure 4A) in the range 0-25% was found in response to activation [5, 44, 76, 77, 79–90]. Simulations showed CMRGlc and $CMRO_2$ time-courses, which are quite in agreement with these figures, albeit a little more pronounced. $CMRO_2$ settles to approximately +44% during stimulation, whereas CMRGlc exhibit a maximum increase of nearly 100% confined to the early phase of neuronal activation with a following plateau near +30% of the baseline (Figures 4A,B). It should be realized that the extent of the uncoupling between CMRGlc and $CMRO_2$ may depend on the experimental paradigm, as suggested by the large range of observed values. Moreover, it is a characteristic of the initial period following neuronal activation, which anticipates the lactate accumulation. Interestingly, the activation-derived uncoupling between CMRGlc and $CMRO_2$ is produced almost exclusively by neurons, as reflected by the oxygen/glucose

index (OGI) time-course (Figure 4C). This is consistent with the predominantly neuronal lactate production and export which result from model simulations (Figures 3A,B). Consistently with neurons as the primary determinant in the focusing of the metabolic response during the early stages of brain activation, it has been observed that the lactate accumulation is accompanied by a similar time-course of the underlying electroencephalographic (EEG) signal power [38]. This claims for a substantial contribution to brain energy metabolism by the electrical activity of neurons, which is also suggested by the observed evolution of microelectrode recordings showing a rapid adaptation of the electrical response [91, 92].

Several alternative interpretations are possible for the reported uncoupling between CMRGlc and $CMRO_2$ during brain activation. The first to be proposed was that the aerobic enzymatic pool may be already saturated at rest, and thus any further energy requirement would be met anaerobically [5, 81]. This would imply a poor energetic cost of neuronal activity with respect to the resting condition (glycolysis produces only 6% of the ATP generated by the complete oxidation of glucose). As this may not be the case [93, 94], saturation of cytochrome oxidase is never observed [95], while it can be more likely a saturation of the oxygen delivery to the brain [96]. The lactate washout, both to the blood and to brain regions outside the activated area (via extracellular space), may contribute to the uncoupling as well. However, drainage of excess lactate has been found to be very small [49, 97]. Scarce endorsement has been reserved also to the so called glycogen shunt mechanism [68], in which glucose taken up during activation would serve to replenish the glycogen content in astrocytes. It is likely that a predominant role in energy usage and allocation is accounted for by the so-called tripartite synapse ultrastructure, where synapse-ensheating pheripheral astrocytic processes (PAPs) are devoid of mitochondria but rich in glycogen [69]. This would allot the relationships between neural activity and metabolism to the synaptic action, while explaining its details by means of structural considerations. On the other hand, the uncoupling can be accounted for by the activation-dependent switch to processes which are primarily served by glycolysis [65], and this would call into attention the electrical activity—i.e. ionic movements—of neurons.

Modeling the brain physiological mechanisms involved in neuronal activation is subjected to a number of limitations. Perhaps, the most severe is the complete lack in quantitative description of intracellular signaling cascades, which are known to have a significant amplification effect on cellular processes [98]. For example, thermodynamic examination of ANLS hypothesis should lead to the conclusion that astrocytic glutamate uptake, which costs only 1-3% of brain ATP, cannot be sufficient to stimulate astrocytic glycolysis and lactate production from glucose [99]. However, astrocytic Ca^{2+}-mediated signaling mechanisms may trigger cellular activities without any obvious metabolic origin [12]. The model also cannot incorporate all brain metabolites and related enzyme-catalyzed reactions, and it can provide necessarily an incomplete description. Most notably, glycogen and glutamate metabolism may play an important role in assessing the exact evolution of metabolites trafficking between neurons and glia. Moreover, even the theoretical account of the included processes is still partial. For example, the specific kinetic properties of lactate dehydrogenase (LDH) isoenzymes, which are differently expressed in neurons and glia, have not been considered. It is worth realizing that energy metabolism is not uniform throughout the brain, and large variations exist between different cortical regions, even at rest [100]. Metabolic variability exists also between different parts of the cell. The subcellular characterization of the energetic supply and demand has been well established for neuronal cells, for which the changes in metabolic rate associated with neuronal activation are localized to regions with high synaptic density in

dendrites, axon terminals, and axonal processes [101–104]. The distribution of mitochondria also points in this direction. Mitochondria are especially abundant in regions having high rate of oxidative metabolism, and their number can rise locally if the energy demand increases, such as during increased activity [105]. Accordingly, the number of mitochondria per unit area in dendrites far outnumber the mitochondrial density in cell body and axon [106]. Cytochrome oxidase activity, which is an indicator of oxidative metabolism, has been found to be particularly intense in areas of the visual cortex corresponding to cellular assemblies having the highest rate of glucose metabolism in response to visual stimulation [107]. Interestingly, the level of cytochrome oxidase staining is greater in dendrites than in soma, and is colocalized with TCA enzyme succinate dehydrogenase, and, most notably, with high densities of Na^+/K^+–ATPase [100]. On the contrary, regions of the brain with high cytochrome oxidase activity have low density of the enzyme lactate dehydrogenase [108–110]. This suggest that regions with high synaptic activity have also a high capacity for oxidative phosphorylation, which may be reflected in the distinct metabolic pattern of neurons and astrocytes, and of their subcellular domains. Thus, it is fundamental to refine the model further on a theoretical account, in order to consider the various neuronal and astrocytic properties at the subcellular level. Oddly, differences arises from the physiologic processes of spiking and synaptic activities which characterize the neural signaling within synapses, dendrites and axons of neurons. It should be realized, however, that subcellular compartmentation exists also in astrocytes, and it is well documented [111–116]. It is likely that astrocytic processes interacting closely with nerve terminals represent a particularly metabolically active compartment [73]. Unfortunately, the information about subcellular *in vivo* energy metabolism is not yet available, and it is difficult to investigate experimentally the highly operative metabolism that takes place in the many lamellar processes of astrocytes, which are intertwined with neuronal structures and interacts with a plenty of synapses [117].

In spite of the all these intrinsic limits, information derived by mathematical modeling may contribute to the understanding of the cerebral metabolic response to stimulation and how this shapes the normal and altered functioning of the brain. Importantly, physiological interpretation of functional imaging techniques may derive great benefit from the modeling approach, at least in emphasizing the lack of knowledge about how exactly these methods relate to brain activity.

In conclusion, we combined several presently available theoretical models of the metabolism and transport of a number of key brain metabolites in order to appreciate the functional significance of glucose and lactate exchanges. We found that (i) glucose is the major energy substrate of neurons, at rest as well as during activation; (ii) shuttled lactate does not provide an important carbon source as compared with glucose taken up by neurons; (iii) a lactate shuttle from neurons to astrocytes is observed in response to neuronal stimulation.

References

[1] Luc Pellerin and Pierre J Magistretti. Food for thought: challenging the dogmas. *Journal of Cerebral Bloood Flow and Metabolism1*, 23(11):1282–1286, Nov 2003.

[2] Claire Peppiatt and David Attwell. Neurobiology: feeding the brain. *Nature*, 431(7005):137–138, Sep 2004.

[3] Siesjo B. *Brain energy metabolism*. Wiley, New York, 1978.

[4] Sokoloff L, Reivich M, Kennedy C, Des Rosiers MH, Patlak CS, Pettigrew KD, Sakurada O, Shinohara M. The [14C]deoxyglucose method for the measurement of local cerebral glucose utilization: theory, procedure, and normal values in the conscious and anesthetized albino rat. *J. Neurochem.*, 28:897–916, 1977.

[5] Fox PT, Raichle ME, Mintun MA, Dence C. Nonoxydative glucose consumption during focal physiologic neural activity. *Science*, 241:462–464, 1988.

[6] Prichard J, Rothman D, Novotny E, Petroff O, Kuwabara T, Avison M, Howseman A, Hanstock C, Shulman R. Lactate rise detected by 1H-NMR in human visual cortex during physiologic stimulation. *Proc Natl Acad Sci USA*, 88:5829–5831, 1991.

[7] L. Pellerin and P.J. Magistretti. Glutamate uptake into astrocytes stimulates aerobic glycolysis: a mechanism coupling neuronal activity to glucose utilization. *Proc Natl Acad Sci USA*, 91:10625–10629, 1994.

[8] Silvia Mangia, Girolamo Garreffa, Marta Bianciardi, Federico Giove, Francesco Di Salle, and Bruno Maraviglia. The aerobic brain: lactate decrease at the onset of neural activity. *Neuroscience*, 118(1):7–10, 2003.

[9] Ching-Ping Chih and Eugene L Roberts Jr. Energy substrates for neurons during neural activity: a critical review of the astrocyte-neuron lactate shuttle hypothesis. *Journal of Cerebral Bloood Flow and Metabolism1*, 23(11):1263–1281, Nov 2003.

[10] A. Aubert and R. Costalat. A model of the coupling between brain electrical activity, metabolism, and hemodynamics: application to the interpretation of functional neuroimaging. *Neuroimage*, 17:1162–1181, 2002.

[11] Agnes Aubert and Robert Costalat. Interaction between astrocytes and neurons studied using a mathematical model of compartmentalized energy metabolism. *Journal of Cerebral Bloood Flow and Metabolism1*, 25(11):1476–1490, Nov 2005.

[12] Ian A Simpson, Anthony Carruthers, and Susan J Vannucci. Supply and demand in cerebral energy metabolism: the role of nutrient transporters. *Journal of Cerebral Bloood Flow and Metabolism*, 27:1766–1791, Jun 2007.

[13] S. Schuster, D. A. Fell, and T. Dandekar. A general definition of metabolic pathways useful for systematic organization and analysis of complex metabolic networks. *Nat. Biotechnol.*, 18(3):326–332, Mar 2000.

[14] Reinhart Heinrich and Stefan Schuster. *The Regulation of Cellular Systems*. Chapman & Hall, 1996.

[15] Francisco Llaneras and JesÃČÂžs PicÃČÂş. Stoichiometric modelling of cell metabolism. *J. Biosci. Bioeng.*, 105(1):1–11, Jan 2008.

[16] Radhakrishnan Mahadevan, Jeremy S Edwards, and Francis J Doyle. Dynamic flux balance analysis of diauxic growth in escherichia coli. *Biophys. J.*, 83(3):1331–1340, Sep 2002.

[17] Ping Ao, Lik Wee Lee, Mary E Lidstrom, Lan Yin, and Xiaomei Zhu. Towards kinetic modeling of global metabolic networks: Methylobacterium extorquens am1 growth as validation. *Sheng Wu Gong Cheng Xue Bao*, 24(6):980–994, Jun 2008.

[18] O. B. Paulson. Blood-brain barrier, brain metabolism and cerebral blood flow. *Eur. Neuropsychopharmacol.*, 12(6):495–501, Dec 2002.

[19] Gertrudis Perea and Alfonso Araque. Communication between astrocytes and neurons: a complex language. *J Physiol Paris*, 96(3-4):199–207, 2002.

[20] Simon B Laughlin and Terrence J Sejnowski. Communication in neuronal networks. *Science*, 301(5641):1870–1874, Sep 2003.

[21] J. Frahm, G. Kruger G, K. D. Merboldt, and A. Kleinschmidt. Dynamic uncoupling and recoupling of perfusion and oxidative metabolism during focal brain activation in man. *Magn Reson Med*, 35:143–148, 1996.

[22] Frahm J, Krueger G, Merboldt KD, Kleinschmidt A. Dynamic NMR studies of perfusion and oxidative metabolism during focal brain activation. *Adv. Exp. Med. Biol.*, 413:195–203, 1997.

[23] Chen W, Novotny EJ, Zhu XH, Rothman DL, Shulman RG. Localized 1H-NMR measurement of glucose consumption in the human brain visual stimulation. *Proc Natl Acad Sci USA*, 90:9896–9900, 1993.

[24] L. K. Fellows, M. G. Boutelle, and M. Fillenz. Extracellular brain glucose levels reflect local neuronal activity: a microdialysis study in awake, freely moving rats. *J Neurochem*, 59(6):2141–2147, Dec 1992.

[25] A. E. Fray, M. Boutelle, and M. Fillenz. Extracellular glucose turnover in the striatum of unanaesthetized rats measured by quantitative microdialysis. *J Physiol*, 504 (Pt 3):721–726, Nov 1997.

[26] E. C. McNay, T. M. Fries, and P. E. Gold. Decreases in rat extracellular hippocampal glucose concentration associated with cognitive demand during a spatial task. *Proc Natl Acad Sci U S A*, 97(6):2881–2885, Mar 2000.

[27] E. C. McNay, R. C. McCarty, and P. E. Gold. Fluctuations in brain glucose concentration during behavioral testing: dissociations between brain areas and between brain and blood. *Neurobiol Learn Mem*, 75(3):325–337, May 2001.

[28] Merboldt KD, Bruhn H, Hanicke W, Michaelis T, Frahm J. Decrease of glucose in the human visual cortex during photic stimulation. *Magn Reson Med*, 25:187–194, 1992.

[29] I. A. Silver and M. EreciÃĔâĂďska. Extracellular glucose concentration in mammalian brain: continuous monitoring of changes during increased neuronal activity and upon limitation in oxygen supply in normo-, hypo-, and hyperglycemic animals. *J Neurosci*, 14(8):5068–5076, Aug 1994.

[30] J. P. Lowry, R. D. O'Neill, M. G. Boutelle, and M. Fillenz. Continuous monitoring of extracellular glucose concentrations in the striatum of freely moving rats with an implanted glucose biosensor. *J Neurochem*, 70(1):391–396, Jan 1998.

[31] G. KrÃĊÂijger, A. Kleinschmidt, and J. Frahm. Dynamic mri sensitized to cerebral blood oxygenation and flow during sustained activation of human visual cortex. *Magn Reson Med*, 35(6):797–800, Jun 1996.

[32] Blomqvist G, Seitz RJ, Sjogren I, Halldin C, Stone-Elander S, Widen L, Solin O, Haaparanta M. Regional cerebral oxidative and total glucose consumption during rest and activation studied with positron emission tomography. *Acta Physiol. Scand.*, 151:29–43, 1994.

[33] L. A. De Bruin, E. M. Schasfoort, A. B. Steffens, and J. Korf. Effects of stress and exercise on rat hippocampus and striatum extracellular lactate. *Am J Physiol*, 259(4 Pt 2):R773–R779, Oct 1990.

[34] Fellows LK, Boutelle MG. Rapid changes in extracellular glucose levels and blood flow in the striatum of the freely moving rat. *Brain Res.*, 604:225–231, 1993.

[35] Fray AE, Forsyth RJ, Boutelle MG, Fillenz M. The mechanisms controlling physiologically stimulated changes in rat brain glucose and lactate: a microdialysis study. *J. Physiol.*, 496:49–57, 1996.

[36] Jenkins BG, Belliveau JW, Rosen BR. Confirmation of lactate production during photic stimulation. Improved protocols using inter– and intra–subject averaging. In *Book of abstracts: 11th annual scientific meeting SMRM*, volume 2, page 2145, 1992.

[37] Menon RS, Gati JS. Two second temporal resolution measurements of lactate correlate with EPI BOLD fMRI timecourses during photic stimulation. In *Book of Proceedings*, page 152, Vancouver, 1997. International Society for Magnetic Resonance in Medicine, 5° Scientific Meeting.

[38] Sappey-Marinier D, Calabrese G, Fein G, Hugg JW, Biggins C, Weiner MW. Effect of photic stimulation on human visual cortex lactate and phosphates using ^{1}H and ^{31}P magnetic resonance spectroscopy. *J Cereb Blood Flow Metab*, 12:584–592, 1992.

[39] M. Ueki, F. Linn, and K. A. Hossmann. Functional activation of cerebral blood flow and metabolism before and after global ischemia of rat brain. *J Cereb Blood Flow Metab*, 8(4):486–494, Aug 1988.

[40] Singh M, Kim H, Huang H, Kim T. Effect of stimulus rate on lactate in the human auditory cortex. In *Book of abstracts: 11th annual scientific meeting SMRM*, volume 2, page 2146, 1992.

[41] Kuwabara T, Watanabe H, Tsuji S, Yuasa T. Lactate rise in the basal ganglia accompanying finger movements: a localized 1H-MRS study. *Brain Res.*, 670:326–328, 1995.

[42] Anna S Urrila, Antti Hakkarainen, Sami Heikkinen, Kim Vuori, Dag Stenberg, Anna-Maija Häkkinen, Nina Lundbom, and Tarja Porkka-Heiskanen. Metabolic imaging of human cognition: an fMRI/^{1}H–MRS study of brain lactate response to silent word generation. *Journal of Cerebral Bloood Flow and Metabolism1*, 23(8):942–948, Aug 2003.

[43] Buxton RB. The elusive initial dip. *Neuroimage*, 13:953–958, 2001.

[44] Hoge RD, Atkinson J, Gill B, Crelier GR, Marrett S, Pike GB. Linear couplig between cerebral blood flow and oxygen consumption in activated human cortex. *Proc Natl Acad Sci USA*, 96:9403–9408, 1999.

[45] Hu YB, Wilson GS. A temporary local energy pool coupled to neuronal activity: fluctuations of extracellular lactate levels in rat brain monitored with rapid-response enzyme-based sensor. *J. Neurochem*, 69:1484–1490, 1997.

[46] E. DÃĊÂżra, L. Gyulai, and A. G. KovÃĊÂżch. Determinants of brain activation-induced cortical nad/nadh responses in vivo. *Brain Res*, 299(1):61–72, May 1984.

[47] C. William Shuttleworth, Angela M Brennan, and John A Connor. Nad(p)h fluorescence imaging of postsynaptic neuronal activation in murine hippocampal slices. *J Neurosci*, 23(8):3196–3208, Apr 2003.

[48] Kasischke KA, Vishwasrao HD, Fisher PJ, Zipfel WR, Webb WW. Neural activity triggers neuronal oxidative metabolism followed by astrocytic glycolysis. *Science*, 305:99–103, 2004.

[49] Albert Gjedde. *Cerebrovascular Disease*, chapter The relation between brain function and cerebral blood flow and metabolism. Lippincott-Raven, Philadelphia, 1997.

[50] Dienel GA, Hertz L. Glucose and lactate metabolism during brain activation. *J. Neruosci. Res.*, 66:824–838, 2001.

[51] Leif Hertz and Gerald A Dienel. Lactate transport and transporters: general principles and functional roles in brain cells. *J Neurosci Res*, 79(1-2):11–18, 2005.

[52] Anne-Karine Bouzier-Sore, Pierre Voisin, Paul Canioni, Pierre J Magistretti, and Luc Pellerin. Lactate is a preferential oxidative energy substrate over glucose for neurons in culture. *J Cereb Blood Flow Metab*, 23(11):1298–1306, Nov 2003.

[53] Nicola J Allen, Ragnhildur KÃČÂąradÃČÂşttir, and David Attwell. A preferential role for glycolysis in preventing the anoxic depolarization of rat hippocampal area ca1 pyramidal cells. *J Neurosci*, 25(4):848–859, Jan 2005.

[54] Lasse K Bak, Arne Schousboe, Ursula Sonnewald, and Helle S Waagepetersen. Glucose is necessary to maintain neurotransmitter homeostasis during synaptic activity in cultured glutamatergic neurons. *Journal of Cerebral Bloood Flow and Metabolism1*, 26(10):1285–1297, Oct 2006.

[55] J. T. Tildon, M. C. McKenna, J. Stevenson, and R. Couto. Transport of l-lactate by cultured rat brain astrocytes. *Neurochem Res*, 18(2):177–184, Feb 1993.

[56] I. A. Silver, J. Deas, and M. EreciÃĚâĂďska. Ion homeostasis in brain cells: differences in intracellular ion responses to energy limitation between cultured neurons and glial cells. *Neuroscience*, 78(2):589–601, May 1997.

[57] Gerald A Dienel, Robert Y Wang, and Nancy F Cruz. Generalized sensory stimulation of conscious rats increases labeling of oxidative pathways of glucose metabolism when the brain glucose-oxygen uptake ratio rises. *J Cereb Blood Flow Metab*, 22(12):1490–1502, Dec 2002.

[58] R. A. Swanson, M. M. Morton, S. M. Sagar, and F. R. Sharp. Sensory stimulation induces local cerebral glycogenolysis: demonstration by autoradiography. *Neuroscience*, 51(2):451–461, Nov 1992.

[59] P. HOROWICZ and M. G. LARRABEE. Glucose consumption and lactate production in a mammalian sympathetic ganglion at rest and in activity. *J Neurochem*, 2(2-3):102–118, 1958.

[60] F. Hyder, J. R. Chase, K. L. Behar, G. F. Mason, M. Siddeek, D. L. Rothman, and R. G. Shulman. Increased tricarboxylic acid cycle flux in rat brain during forepaw stimulation detected with 1h[13c]nmr. *Proc Natl Acad Sci U S A*, 93(15):7612–7617, Jul 1996.

[61] M. G. LARRABEE. Oxygen consumption of excised sympathetic ganglia at rest and in activity. *J. Neurochem.*, 2(2-3):81–101, 1958.

[62] Malonek D, Grinvald A. Interactions between electrical activity and cortical microcirculation revealed by imaging spectroscopy: implications for functional brain mapping. *Science*, 272:551–554, 1996.

[63] J. M. Ritchie. The oxygen consumption of mammalian non-myelinated nerve fibres at rest and during activity. *J Physiol*, 188(3):309–329, Feb 1967.

[64] M. Barinaga. What makes brain neurons run? *Science*, 276(5310):196–198, Apr 1997.

[65] A. Ames. CNS energy metabolism as related to function. *Brain Res Brain Res Rev*, 34(1-2):42–68, Nov 2000.

[66] Avital Schurr. Lactate: the ultimate cerebral oxidative energy substrate? *Journal of Cerebral Bloood Flow and Metabolism1*, 26(1):142–152, Jan 2006.

[67] Gerald A Dienel and Nancy F Cruz. Nutrition during brain activation: does cell-to-cell lactate shuttling contribute significantly to sweet and sour food for thought? *Neurochem Int*, 45(2-3):321–351, 2004.

[68] R. G. Shulman, F. Hyder, and D. L. Rothman. Cerebral energetics and the glycogen shunt: neurochemical basis of functional imaging. *Proc Natl Acad Sci U S A*, 98(11):6417–6422, May 2001.

[69] Leif Hertz, Liang Peng, and Gerald A Dienel. Energy metabolism in astrocytes: high rate of oxidative metabolism and spatiotemporal dependence on glycolysis/glycogenolysis. *Journal of Cerebral Bloood Flow and Metabolism1*, 27(2):219–249, Feb 2007.

[70] Ditte Lovatt, Ursula Sonnewald, Helle S Waagepetersen, Arne Schousboe, Wei He, Jane H-C Lin, Xiaoning Han, Takahiro Takano, Su Wang, Fraser J Sim, Steven A Goldman, and Maiken Nedergaard. The transcriptome and metabolic gene signature of protoplasmic astrocytes in the adult murine cortex. *J Neurosci*, 27(45):12255–12266, Nov 2007.

[71] Mauro DiNuzzo, Silvia Mangia, Bruno Maraviglia, and Federico Giove. Changes in glucose uptake rather than lactate shuttle take center stage in subserving neuroenergetics: evidence from mathematical modeling. *J Cereb Blood Flow Metab*, in print, doi:10.1038/jcbfm.2009.232.

[72] Federico Giove, Silvia Mangia, Marta Bianciardi, Girolamo Garreffa, Francesco Di Salle, Renato Morrone, and Bruno Maraviglia. The physiology and metabolism of neuronal activation: "in vivo" studies by NMR and other methods. *Magn Reson Imaging*, 21:1283–1293, 2003.

[73] Gerald A Dienel and Nancy F Cruz. Neighborly interactions of metabolically-activated astrocytes in vivo. *Neurochem Int*, 43(4-5):339–354, 2003.

[74] Pawlik G and Heiss WD. *Neuropsychological Function and Brain Imaging*, chapter Positron emission tomography and neurophysiological function. Plenum Press, New York, 1989.

[75] L. Sokoloff. Localization of functional activity in the central nervous system by measurement of glucose utilization with radioactive deoxyglucose. *J Cereb Blood Flow Metab*, 1(1):7–36, 1981.

[76] Roland PE, Eriksson L, Stone-Elander S, Widen L. Does mental activity change the oxydative metabolism of the brain? *J. Neurosci.*, 7:2373–2389, 1987.

[77] Seitz RJ, Roland PE. Vibratory stimulation increases and decreases the regional cerebral blood flow and oxydative metabolism: a positron emission tomography (PET) study. *Acta Neurol. Scand.*, 86:60–67, 1992.

[78] P. L. Madsen, S. Holm, M. Herning, and N. A. Lassen. Average blood flow and oxygen uptake in the human brain during resting wakefulness: a critical appraisal of the kety-schmidt technique. *J Cereb Blood Flow Metab*, 13(4):646–655, Jul 1993.

[79] Ribeiro L, Kuwabara H, Meyer E, Fujita H, Marrett S, Evans AC, and Gjedde A. Cerebral blood flow and metabolysm during nonspecific bilateral visual stimulation in normal subjects. In K. Uemura and others, editor, *Quantification of brain function. Tracer kinetics and image analysis in brain PET*, pages 229–234, Amsterdam, 1993. Elsevier Science Publication.

[80] Madsen PL, Hasselbalch SG, Hagemann LP, Olsen KS, Bulow J, Holm S, Wildschiodtz G, Paulson OB, Lassen NA. Persistent resetting of the cerebral oxygen/glucose uptake ratio by brain activation: evidence obtained with the Kety–Schmidt technique. *J Cereb Blood Flow Metab*, 15:485–491, 1995.

[81] Fox PT, Raichle ME. Focal physiological uncoupling of cerebral blood flow and oxidative metabolism during somatosensory stimulation in human subjects. *Proc Natl Acad Sci USA*, 83:1140–1144, 1986.

[82] Marrett S *et al.* Stimulus specific increase of oxidative metabolism in human visual cortex. In K. Uemura and others, editor, *Quantification of brain function. Tracer kinetics and image analysis in brain PET*, pages 217–224, Amsterdam, 1993. Elsevier Science Publication.

[83] Marrett S. *et al.* Differential increases of oxygen metabolism in visual cortex. *J Cereb Blood Flow Metab*, 15 (suppl. 1):S80, 1995.

[84] Marrett S, Gjeddie A. Changes of blood flow and oxygen consumption in visual cortex of living humans. In A. Villringer and others, editor, *Optical Imaging of Brain Function and Metabolism II*, pages 205–208, New York, 1997. Plenum Press.

[85] Kim SG, Uğurbil K. Comparison of blood oxygenation and cerebral blood flow effects in fMRI: estimation of relative oxygen consumption change. *Magn Reson Med*, 38:59–65, 1997.

[86] T.L. Davis, K.K. Kwong, R.M. Weisskoff, and B.R. Rosen. Calibrated functional MRI: mapping the dynamics of oxidative metabolism. *Proc Natl Acad Sci USA*, 95:1834–1839, 1998.

[87] Vafaee MS, Marrett S, Meyer E, Evans AC, Gjedde A. Increased oxygen consumption in human visual cortex: response to visual stimulation. *Acta Neurol. Scand.*, 98:85–89, 1998.

[88] Schwarzbauer C, Heinke W. Investigating the dependence of BOLD contrast on oxidative metabolism. *Magn Reson Med*, 41:537–543, 1999.

[89] Kim SG, Rostrup E, Larsson HB, Ogawa S, Paulson OB. Determination of relative CMR_{O_2} from CBF and BOLD changes: significant increase of oxygen consumption rate during visual stimulation. *Magn Reson Med*, 41:1152–1161, 1999.

[90] Kastrup A, Kruger G, Glover GH, Moseley ME. Assessment of cerebral oxidative metabolism with breath holding and fMRI. *Magn Reson Med*, 42:608–611, 1999.

[91] Nikos K. Logothetis, J. Pauls, M. Augath, T. Trinath, and A. Oeltermann. Neurophysiological investigation of the basis of the fMRI signal. *Nature*, 412:150–157, 2001.

[92] Ahalya Viswanathan and Ralph D Freeman. Neurometabolic coupling in cerebral cortex reflects synaptic more than spiking activity. *Nat. Neurosci.*, 10(10):1308–1312, Oct 2007.

[93] Attwell D, Laughlin SB. An Energy Budget for Signaling in the Grey Matter of the Brain. *J Cereb Blood Flow Metab*, 21:1133–1145, 2001.

[94] Peter Lennie. The cost of cortical computation. *Curr. Biol.*, 13(6):493–497, Mar 2003.

[95] K. F. LaNoue, F. M. Jeffries, and G. K. Radda. Kinetic control of mitochondrial atp synthesis. *Biochemistry*, 25(23):7667–7675, Nov 1986.

[96] Buxton RB, Frank LR. A model for the coupling between cerebral blood flow and oxygen metabolism during neural stimulation. *J Cereb Blood Flow Metab*, 17:64–72, 1997.

[97] WG Kuhr and J Korf. Extracellular lactic acid as an indicator of brain metabolism: continuous online measurement in conscious, freely moving rats. *J Cereb Blood Flow Metab*, 8:130–137, 1988.

[98] D L Nelson and M M Cox. *Lehninger Principles of Biochemistry*. W.H.Freeman & Company, New York, 2008.

[99] Marianne Fillenz. The role of lactate in brain metabolism. *Neurochem. Int.*, 47(6):413–417, Nov 2005.

[100] Per E. Roland. *Brain Activation*. Wiley-Liss, New York, 1993.

[101] S. L. Juliano, P. J. Hand, and B. L. Whitsel. Patterns of increased metabolic activity in somatosensory cortex of monkeys macaca fascicularis, subjected to controlled cutaneous stimulation: a 2-deoxyglucose study. *J Neurophysiol*, 46(6):1260–1284, Dec 1981.

[102] S. L. Juliano, P. J. Hand, and B. L. Whitsel. Patterns of metabolic activity in cytoarchitectural area sii and surrounding cortical fields of the monkey. *J Neurophysiol*, 50(4):961–980, Oct 1983.

[103] M. Kadekaro, A. M. Crane, and L. Sokoloff. Differential effects of electrical stimulation of sciatic nerve on metabolic activity in spinal cord and dorsal root ganglion in the rat. *Proc Natl Acad Sci U S A*, 82(17):6010–6013, Sep 1985.

[104] W. J. Schwartz, C. B. Smith, L. Davidsen, H. Savaki, L. Sokoloff, M. Mata, D. J. Fink, and H. Gainer. Metabolic mapping of functional activity in the hypothalamo-neurohypophysial system of the rat. *Science*, 205(4407):723–725, Aug 1979.

[105] M. EreciÃĚâĂďska and D. F. Wilson. Regulation of cellular energy metabolism. *J Membr Biol*, 70(1):1–14, 1982.

[106] M. T. Wong-Riley. Cytochrome oxidase: an endogenous metabolic marker for neuronal activity. *Trends Neurosci*, 12(3):94–101, Mar 1989.

[107] M. S. Livingstone and D. H. Hubel. Anatomy and physiology of a color system in the primate visual cortex. *J Neurosci*, 4(1):309–356, Jan 1984.

[108] R. L. FRIEDE, L. M. FLEMING, and M. KNOLLER. A comparative mapping of enzymes involved in hexosemonophosphate shunt and citric acid cycle in the brain. *J Neurochem*, 10:263–277, Apr 1963.

[109] I. W. Borowsky and R. C. Collins. Metabolic anatomy of brain: a comparison of regional capillary density, glucose metabolism, and enzyme activities. *J Comp Neurol*, 288(3):401–413, Oct 1989.

[110] R. C. Collins. Basic aspects of functional brain metabolism. *Ciba Found Symp*, 163:6–16; discussion 16–22, 1991.

[111] Berl S, Clarke DD, and Schneider D, editors. *Metabolic Compartmentation and Neurotransmission: Relation to Brain Structure and Function*. Plenum Press, New York, 1975.

[112] L. Hertz, R. Dringen, A. Schousboe, and S. R. Robinson. Astrocytes: glutamate producers for neurons. *J Neurosci Res*, 57(4):417–428, Aug 1999.

[113] A. Schousboe, N. Westergaard, U. Sonnewald, S. B. Petersen, R. Huang, L. Peng, and L. Hertz. Glutamate and glutamine metabolism and compartmentation in astrocytes. *Dev Neurosci*, 15(3-5):359–366, 1993.

[114] H. Wiesinger, B. Hamprecht, and R. Dringen. Metabolic pathways for glucose in astrocytes. *Glia*, 21(1):22–34, Sep 1997.

[115] A. Schousboe, Ursula Sonnewald, and Helle S Waagepetersen. Differential roles of alanine in gabaergic and glutamatergic neurons. *Neurochem Int*, 43(4-5):311–315, 2003.

[116] M. C. McKenna, J. T. Tildon, R. Couto, J. H. Stevenson, and F. J. Caprio. The metabolism of malate by cultured rat brain astrocytes. *Neurochem Res*, 15(12):1211–1220, Dec 1990.

[117] M. C. McKenna, R. Gruetter, U. Sonnewald, H. S. Waagepetersen, and A. Schousboe. *Basic Neurochemistry*, chapter Energy metabolism of the brain. Elsevier Academic Press, 2006.

[118] A. Aubert, R. Costalat, and R. Valabrègue. Modelling of the coupling between brain electrical activity and metabolism. *Acta Biotheor*, 49(4):301–326, 2001.

[119] A. L. HODGKIN and P. HOROWICZ. The influence of potassium and chloride ions on the membrane potential of single muscle fibres. *J Physiol*, 148:127–160, Oct 1959.

[120] D. D. Clarke and L. Sokoloff. *Basic Neurochemistry*, chapter Circulation and energy metabolism of the brain. Lippincott Williams & Wilkins, Philadelphia, 1999.

[121] T. Wallimann, M. Wyss, D. Brdiczka, K. Nicolay, and H. M. Eppenberger. Intracellular compartmentation, structure and function of creatine kinase isoenzymes in tissues with high and fluctuating energy demands: the 'phosphocreatine circuit' for cellular energy homeostasis. *Biochem. J.*, 281 (Pt 1):21–40, Jan 1992.

[122] O. H. LOWRY and J. V. PASSONNEAU. The relationships between substrates and enzymes of glycolysis in brain. *J. Biol. Chem.*, 239:31–42, Jan 1964.

[123] T. A. Rapoport, R. Heinrich, and S. M. Rapoport. The regulatory principles of glycolysis in erythrocytes in vivo and in vitro. a minimal comprehensive model describing steady states, quasi-steady states and time-dependent processes. *Biochem. J.*, 154(2):449–469, Feb 1976.

[124] R. A. Meyer, H. L. Sweeney, and M. J. Kushmerick. A simple analysis of the "phosphocreatine shuttle". *Am. J. Physiol.*, 246(5 Pt 1):C365–C377, May 1984.

[125] S. N. Fedosov. Creatine-creatine phosphate shuttle modeled as two-compartment system at different levels of creatine kinase activity. *Biochim. Biophys. Acta*, 1208(2):238–246, Oct 1994.

[126] M. K. Aliev and V. A. Saks. Compartmentalized energy transfer in cardiomyocytes: use of mathematical modeling for analysis of in vivo regulation of respiration. *Biophys. J.*, 73(1):428–445, Jul 1997.

[127] Masanori Tachikawa, Ken-Ichi Hosoya, Sumio Ohtsuki, and Tetsuya Terasaki. A novel relationship between creatine transport at the blood-brain and blood-retinal barriers, creatine biosynthesis, and its use for brain and retinal energy homeostasis. *Subcell Biochem*, 46:83–98, 2007.

[128] Masanori Tachikawa, Masahiro Fukaya, Tetsuya Terasaki, Sumio Ohtsuki, and Masahiko Watanabe. Distinct cellular expressions of creatine synthetic enzyme gamt and creatine kinases uck-mi and ck-b suggest a novel neuron-glial relationship for brain energy homeostasis. *Eur J Neurosci*, 20(1):144–160, Jul 2004.

[129] Lubert Stryer. *Biochemistry*. W.H.Freeman, New York, 1995.

[130] T. A. Rapoport and R. Heinrich. Mathematical analysis of multienzyme systems. i. modelling of the glycolysis of human erythrocytes. *Biosystems*, 7(1):120–129, Jul 1975.

[131] R. Heinrich and T. A. Rapoport. Mathematical analysis of multienzyme systems. ii. steady state and transient control. *Biosystems*, 7(1):130–136, Jul 1975.

[132] P. G. Bittar, Y. Charnay, L. Pellerin, C. Bouras, and P. J. Magistretti. Selective distribution of lactate dehydrogenase isoenzymes in neurons and astrocytes of human brain. *J Cereb Blood Flow Metab*, 16(6):1079–1089, Nov 1996.

[133] G. J. Kemp. Non-invasive methods for studying brain energy metabolism: what they show and what it means. *Dev Neurosci*, 22(5-6):418–428, 2000.

[134] David Attwell and Costantino Iadecola. The neural basis of functional brain imaging signals. *Trends Neurosci.*, 25(12):621–625, Dec 2002.

[135] Buxton RB, Wong EC, Frank LR. Dynamics of blood flow and oxygenation changes during brain activation: the balloon model. *Magn Reson Med*, 39:855–864, 1998.

[136] R. Gruetter, K. Ugurbil, and E. R. Seaquist. Steady-state cerebral glucose concentrations and transport in the human brain. *J. Neurochem.*, 70(1):397–408, Jan 1998.

[137] F J Thomson and G W Gould. *Facilitative Glucose Transporters*, chapter Regulation of glucose transport by growth factors and oncogenes. R. G. Landes Company, Austin TX, 1997.

[138] Luc Leybaert, Marijke De Bock, Marijke Van Moorhem, Elke Decrock, and Elke De Vuyst. Neurobarrier coupling in the brain: adjusting glucose entry with demand. *J. Neurosci. Res.*, 85(15):3213–3220, Nov 2007.

[139] A W Vorbrodt. *The Blood-Brain Barrier*, chapter Morphological evidence of the functional polarization of brain microvascular endothelium. Raven Press, New York, 1993.

[140] R. N. Frank, S. Dutta, and M. A. Mancini. Pericyte coverage is greater in the retinal than in the cerebral capillaries of the rat. *Invest Ophthalmol Vis Sci*, 28(7):1086–1091, Jul 1987.

[141] M. W. Brightman and T. S. Reese. Junctions between intimately apposed cell membranes in the vertebrate brain. *J. Cell Biol.*, 40(3):648–677, Mar 1969.

[142] Sabina HrabetovÃČÆŠÃĆÂą and Charles Nicholson. Contribution of dead-space microdomains to tortuosity of brain extracellular space. *Neurochem. Int.*, 45(4):467–477, Sep 2004.

[143] M. S. Vafaee and A. Gjedde. Model of blood-brain transfer of oxygen explains nonlinear flow-metabolism coupling during stimulation of visual cortex. *Journal of Cerebral Bloood Flow and Metabolism1*, 20(4):747–754, Apr 2000.

A   Appendix

The model consists of coupled ordinary differential equations (Table 1) as time-derivatives of brain metabolites, each of which is subject to several biochemical processes described by rate equations (Table 2) supported by the relevant parameter values (Table 3).

Table 1: Balance equations for brain metabolites and their steady-state concentrations.

Metabolite	Concentration (mM)	Balance equation
Neuron		
Glucose (GLC_n)	1.41	$d[GLC_n]/dt = j_{GLC}^{in} - v_{HKPFK}^{n}$
Glyceraldehyde-3-phosphate (GAP_n)	0.0055	$d[GAP_n]/dt = 2v_{HKPFK}^{n} - v_{PGK}^{n}$
Phosphoenolpyruvate (PEP_n)	0.0188	$d[PEP_n]/dt = v_{PGK}^{n} - v_{PK}^{n}$
Pyruvate (PYR_n)	0.162	$d[PYR_n]/dt = v_{PK}^{n} - v_{LDH}^{n} - v_{Mito}^{n}$
Lactate (LAC_n)	1.04	$d[LAC_n]/dt = v_{LDH}^{n} + j_{LAC}^{in}$
Nicotinamide adenine dinucleotide ($NADH_n$)	0.0267	$d[NADH_n]/dt = v_{PGK}^{n} - v_{LDH}^{n} - v_{Mito}^{n}$
Adenosine triphosphate (ATP_n)	2.2	$d[ATP_n]/dt = (-2v_{HKPFK}^{n} + v_{PGK}^{n} + v_{PK}^{n} - v_{ATPases}^{n} - v_{Pump}^{n} + 15v_{Mito}^{n} + v_{CK}^{n})(1 - dAMP_n/dATP_n)^{-1}$
Sodium (Na_n^+)	14.96	$d[Na_n^+]/dt = v_{Leak-Na}^{n} - 3v_{Pump}^{n} + v_{Stim}^{n}$
Phosphocreatine (PCr_n)	5.01	$d[PCr_n]/dt = -v_{CK}^{n}$
Oxygen (O_{2n})	0.0268	$d[O_{2n}]/dt = j_{O2}^{cn} - 3v_{Mito}^{n}$
Astrocyte		
Glucose (GLC_g)	1.03	$d[GLC_g]/dt = j_{GLC}^{bg} - (V_i/V_g)j_{GLC}^{gi} - v_{HKPFK}^{g}$
Glyceraldehyde-3-phosphate (GAP_g)	0.0054	$d[GAP_g]/dt = 2v_{HKPFK}^{g} - v_{PGK}^{g}$
Phosphoenolpyruvate (PEP_g)	0.0185	$d[PEP_g]/dt = v_{PGK}^{g} - v_{PK}^{g}$
Pyruvate (PYR_g)	0.16	$d[PYR_g]/dt = v_{PK}^{g} - v_{LDH}^{g} - v_{Mito}^{g}$
Lactate (LAC_g)	1.02	$d[LAC_g]/dt = v_{LDH}^{g} + j_{LAC}^{bg} - (V_i/V_g)j_{LAC}^{gi}$
Nicotinamide adenine dinucleotide ($NADH_g$)	0.0264	$d[NADH_g]/dt = v_{PGK}^{g} - v_{LDH}^{g} - v_{Mito}^{g}$
Adenosine triphosphate (ATP_g)	2.2	$d[ATP_g]/dt = (-2v_{HKPFK}^{g} + v_{PGK}^{g} + v_{PK}^{g} - v_{ATPases}^{g} - v_{Pump}^{g} + 15v_{Mito}^{g} + v_{CK}^{g})(1 - dAMP_g/dATP_g)^{-1}$
Sodium (Na_g^+)	15.91	$d[Na_g^+]/dt = v_{Leak-Na}^{g} - 3v_{Pump}^{g} + v_{Stim}^{g}$
Phosphocreatine (PCr_g)	5.02	$d[PCr_g]/dt = -v_{CK}^{g}$
Oxygen (O_{2g})	0.0251	$d[O_{2g}]/dt = j_{O2}^{cg} - 3v_{Mito}^{g}$
Interstitium		
Glucose (GLC_i)	1.53	$d[GLC_i]/dt = j_{GLC}^{gi} + j_{GLC}^{bi} - (V_n/V_i)j_{GLC}^{in}$
Lactate (LAC_i)	1.02	$d[LAC_i]/dt = j_{LAC}^{gi} + j_{LAC}^{bi} - (V_n/V_i)j_{LAC}^{in}$
Capillary		
Glucose (GLC_c)	4.78	$d[GLC_c]/dt = j_{GLC}^{c} - (V_c/V_e)j_{GLC}^{ce}$
Lactate (LAC_c)	0.31	$d[LAC_c]/dt = j_{LAC}^{c} - (V_c/V_e)j_{LAC}^{ce}$
Oxygen (O_{2c})	6.98	$d[O_{2c}]/dt = j_{O2}^{c} - (V_n/V_c)j_{O2}^{cn} - (V_g/V_c)j_{O2}^{cg}$
Endothelium		
Glucose (GLC_e)	3.77	$d[GLC_e]/dt = j_{GLC}^{ce} - (V_b/V_e)j_{GLC}^{eb}$
Lactate (LAC_e)	0.56	$d[LAC_e]/dt = j_{LAC}^{ce} - (V_b/V_e)j_{LAC}^{eb}$
Basal lamina		
Glucose (GLC_b)	2.73	$d[GLC_b]/dt = j_{GLC}^{eb} - (V_i/V_b)j_{GLC}^{bi} - (V_g/V_b)j_{GLC}^{bg}$
Lactate (LAC_b)	0.93	$d[LAC_b]/dt = j_{LAC}^{eb} - (V_i/V_b)j_{LAC}^{bi} - (V_g/V_b)j_{LAC}^{bg}$

A.1   Housekeeping

At rest, nearly half of the ATP production is expended by ATPases other than the sodium pump [49], whose overall contribution $v_{ATPases}$ can be assumed to be constant [118]. This residual metabolism is the result of biochemical processes which provide the basics necessary for cellular life, including vegetative

metabolism, intracellular signaling, and the synthesis of proteins, lipids and nucleotides. A fair part of the brain housekeeping metabolism is used for the axonal transport of substances in neurons. Since neurons seems to have also a relatively higher degree of biosynthetic activity than astrocytes [100], their energy consumption due to housekeeping is thought to be appreciably higher [11], although astrocytic resting energy demand encompasses several processes not readily quantifiable such as filopodial motility [69].

Table 2: Rate equations for reaction/transport mechanisms.

Reaction or transport	Rate equation
Sodium leakage current	$v_{\text{Leak}-\text{Na}}^{\text{x}} = \frac{S_m g_{\text{Na}}^{\text{x}}}{V_x F} \left(\frac{RT}{F} \ln \frac{[\text{Na}_i^+]}{[\text{Na}_x^+]} - V_m \right)$
$\text{Na}^+/\text{K}^+-\text{ATPase}$	$v_{\text{Pump}}^{\text{x}} = \frac{S_m}{V_x} k_{\text{Pump}} [\text{ATP}_x][\text{Na}_x^+] \left(1 + \frac{[\text{ATP}_x]}{K_{m,\text{Pump}}} \right)^{-1}$
Sodium influx due to stimulation	$v_{\text{Stim}}^{\text{x}}(t) = v_1^{\text{x}} + v_2^{\text{x}} \frac{t}{\tau_{\text{Stim}}^{\text{x}}} \exp\left(-\frac{t}{\tau_{\text{Stim}}^{\text{x}}} \right)$
Hexokinase-Phosphofructokinase	$v_{\text{HKPFK}}^{\text{x}} = k_{\text{HKPFK}}^{\text{x}} [\text{ATP}_x] \left[1 + \left(\frac{[\text{ATP}_x]}{K_{I,\text{ATP}}} \right)^{nH} \right]^{-1} \left(1 + \frac{K_g}{[\text{GLC}_x]} \right)^{-1}$
Phosphoglycerate kinase	$v_{\text{PGK}}^{\text{x}} = k_{\text{PGK}}^{\prime \text{x}} [\text{GAP}_x][\text{ADP}_x] \frac{[\text{NAD}_x^+]}{[\text{NADH}_x]}$
Pyruvate kinase	$v_{\text{PK}}^{\text{x}} = k_{\text{PK}}^{\text{x}} [\text{PEP}_x][\text{ADP}_x]$
Lactate dehydrogenase	$v_{\text{LDH}}^{\text{x}} = k_{\text{LDH}}^{\text{x}+} [\text{PYR}_x][\text{NADH}_x] - k_{\text{LDH}}^{\text{x}-} [\text{LAC}_x][\text{NAD}_x^+]$
Mitochondrial respiration	$v_{\text{Mito}}^{\text{x}} = V_{max,\text{Mito}}^{\text{x}} \left(1 + \frac{K_{m,\text{Mito}}}{[\text{PYR}_x]} \right)^{-1} \left(1 + \frac{K_{m,\text{O2}}}{[\text{O}_{2x}]} \right)^{-1} \left(1 + \frac{K_{m,\text{ADP}}^{\text{x}}}{[\text{ADP}_x]} \right)^{-1}$
ATPases	$v_{\text{ATPases}}^{\text{n}} = 0.137 \text{ mmol/L/sec} \qquad v_{\text{ATPases}}^{\text{g}} = 0.094 \text{ mmol/L/sec}$
Creatine kinase	$v_{\text{CK}}^{\text{x}} = k_{\text{CK}}^{+\text{x}} [\text{PCr}_x][\text{ADP}_x] - k_{\text{CK}}^{-\text{x}} [\text{Cr}_x][\text{ATP}_x]$
Blood flow through capillary	$CBF(t) = \begin{cases} CBF_0 \\ (1 + \alpha_F) CBF_0 \end{cases}$
Capillary glucose variation	$j_{\text{GLC}}^{\text{c}} = 2CBF(t) ([\text{GLC}_a] - [\text{GLC}_c])$
Capillary lactate variation	$j_{\text{LAC}}^{\text{c}} = 2CBF(t) ([\text{LAC}_a] - [\text{LAC}_c])$
Capillary oxygen variation	$j_{\text{O2}}^{\text{c}} = 2CBF(t) ([\text{O}_{2a}] - [\text{O}_{2c}])$
Oxygen exchange between blood and tissue	$j_{\text{O2}}^{\text{cx}} = \frac{PSc}{V_x} \left[K_{\text{O2}} \left(\frac{[\text{Hb}]OP_{\text{Hb}}}{[\text{O}_{2c}]} \right)^{-1/nh} - [\text{O}_{2x}] \right]$
Glucose exchange between blood and endothelium	$j_{\text{GLC}}^{\text{ce}} = \frac{T_{max,\text{GLC}}^{\text{ce}}([\text{GLC}_a](K_{eG}+[\text{GLC}_e]) - [\text{GLC}_e](K_{eG}+[\text{GLC}_a]))}{K_{eG}^2 R_{eG,oo} + K_{eG} R_{eG,oi}[\text{GLC}_a] + K_{eG} R_{eG,io}[\text{GLC}_e] + R_{eG,ee}[\text{GLC}_a][\text{GLC}_e]}$
Lactate exchange between blood and endothelium	$j_{\text{LAC}}^{\text{ce}} = \frac{T_{max,\text{LAC}}^{\text{ce}}([\text{LAC}_a][\text{H}^+](K_{eL}+[\text{H}^+][\text{LAC}_e]) - [\text{LAC}_e][\text{H}^+](K_{eL}+[\text{LAC}_a]))}{K_{eL}^2 R_{eL,oo} + K_{eL} R_{eL,oi}[\text{LAC}_a] + K_{eL} R_{eL,io}[\text{LAC}_e] + R_{eL,ee}[\text{LAC}_a][\text{LAC}_e]}$
Glucose exchange between endothelium and basal lamina	$j_{\text{GLC}}^{\text{eb}} = \frac{T_{max,\text{GLC}}^{\text{eb}}([\text{GLC}_e](K_{eG}+[\text{GLC}_b]) - [\text{GLC}_b](K_{eG}+[\text{GLC}_e]))}{K_{eG}^2 R_{eG,oo} + K_{eG} R_{eG,oi}[\text{GLC}_b] + K_{eG} R_{eG,io}[\text{GLC}_e] + R_{eG,ee}[\text{GLC}_e][\text{GLC}_b]}$
Lactate exchange between endothelium and basal lamina	$j_{\text{LAC}}^{\text{eb}} = \frac{T_{max,\text{LAC}}^{\text{eb}}([\text{LAC}_e][\text{H}^+](K_{eL}+[\text{H}^+][\text{LAC}_b]) - [\text{LAC}_b][\text{H}^+](K_{eL}+[\text{LAC}_e]))}{K_{eL}^2 R_{eL,oo} + K_{eL} R_{eL,oi}[\text{LAC}_b] + K_{eL} R_{eL,io}[\text{LAC}_e] + R_{eL,ee}[\text{LAC}_e][\text{LAC}_b]}$
Glucose exchange between basal lamina and astrocyte	$j_{\text{GLC}}^{\text{bg}} = \frac{T_{max,\text{GLC}}^{\text{bg}}([\text{GLC}_b](K_{gG}+[\text{GLC}_g]) - [\text{GLC}_g](K_{gG}+[\text{GLC}_b]))}{K_{gG}^2 R_{bgG,oo} + K_{gG} R_{bgG,oi}[\text{GLC}_b] + K_{gG} R_{bgG,io}[\text{GLC}_g] + R_{bgG,ee}[\text{GLC}_g][\text{GLC}_b]}$
Lactate exchange between basal lamina and astrocyte	$j_{\text{LAC}}^{\text{bg}} = \frac{T_{max,\text{LAC}}^{\text{bg}}([\text{LAC}_b][\text{H}^+](K_{gL}+[\text{LAC}_g][\text{H}^+]) - [\text{LAC}_g][\text{H}^+](K_{gL}+[\text{LAC}_b][\text{H}^+]))}{K_{gL}^2 R_{bgL,oo} + K_{gL} R_{bgL,oi}[\text{LAC}_b][\text{H}^+] + K_{gL} R_{bgL,io}[\text{LAC}_g][\text{H}^+] + R_{bgL,ee}[\text{LAC}_b][\text{LAC}_g][\text{H}^+]^2}$
Glucose diffusion between basal lamina and interstitium	$j_{\text{GLC}}^{\text{bi}} = k_{Diff,\text{GLC}}^{\text{bi}} ([\text{GLC}_b] - [\text{GLC}_i])$
Lactate diffusion between basal lamina and interstitium	$j_{\text{LAC}}^{\text{bi}} = k_{Diff,\text{LAC}}^{\text{bi}} ([\text{LAC}_b] - [\text{LAC}_i])$
Glucose exchange between astrocyte and interstitium	$j_{\text{GLC}}^{\text{gi}} = \frac{T_{max,\text{GLC}}^{\text{gi}}([\text{GLC}_g](K_{gG}+[\text{GLC}_i]) - [\text{GLC}_i](K_{gG}+[\text{GLC}_g]))}{K_{gG}^2 R_{giG,oo} + K_{gG} R_{giG,oi}[\text{GLC}_i] + K_{gG} R_{giG,io}[\text{GLC}_g] + R_{giG,ee}[\text{GLC}_g][\text{GLC}_i]}$
Lactate exchange between astrocyte and interstitium	$j_{\text{LAC}}^{\text{gi}} = \frac{T_{max,\text{LAC}}^{\text{gi}}([\text{LAC}_g][\text{H}^+](K_{gL}+[\text{LAC}_i][\text{H}^+]) - [\text{LAC}_i][\text{H}^+](K_{gL}+[\text{LAC}_g][\text{H}^+]))}{K_{gL}^2 R_{giL,oo} + K_{gL} R_{giL,oi}[\text{LAC}_i][\text{H}^+] + K_{gL} R_{giL,io}[\text{LAC}_g][\text{H}^+] + R_{giL,ee}[\text{LAC}_g][\text{LAC}_i][\text{H}^+]^2}$
Glucose exchange between interstitium and neuron	$j_{\text{GLC}}^{\text{in}} = \frac{T_{max,\text{GLC}}^{\text{in}}([\text{GLC}_i](K_{nG}+[\text{GLC}_n]) - [\text{GLC}_n](K_{nG}+[\text{GLC}_i]))}{K_{nG}^2 R_{nG,oo} + K_{nG} R_{nG,oi}[\text{GLC}_i] + K_{nG} R_{nG,io}[\text{GLC}_n] + R_{nG,ee}[\text{GLC}_n][\text{GLC}_i]}$
Lactate exchange between interstitium and neuron	$j_{\text{LAC}}^{\text{in}} = \frac{T_{max,\text{LAC}}^{\text{in}}([\text{LAC}_i][\text{H}^+](K_{nL}+[\text{LAC}_n][\text{H}^+]) - [\text{LAC}_n][\text{H}^+](K_{nL}+[\text{LAC}_i][\text{H}^+]))}{K_{nL}^2 R_{nL,oo} + K_{nL} R_{nL,oi}[\text{LAC}_i][\text{H}^+] + K_{nL} R_{nL,io}[\text{LAC}_n][\text{H}^+] + R_{nL,ee}[\text{LAC}_n][\text{LAC}_i][\text{H}^+]^2}$

Note that x is either n (neuronal) or g (astroglial).

A.2 Sodium leakage

Active pumping of sodium and potassium against their electrochemical gradients is needed to balance ionic leakage currents, which are given, according to ohmic hypothesis, by the difference between the membrane potential and Nernst potentials [118, 119]. Every sodium ion which enters the cell has to be pumped outside by the $\text{Na}^+/\text{K}^+-\text{ATPase}$, whose stoichiometry involves the ATP-dependent countertransport of 3 Na^+ for 2 K^+. It should be realized that many cellular processes are coupled *de facto* with the sodium pump, even though they do not entail any sodium or potassium movement directly. For example, excess cytosolic Ca^{2+} is in part removed by the $\text{Na}^+/\text{Ca}^{2+}$ exchanger, which benefit of the sodium concentration gradient. The uneven sodium distribution across plasma membrane is also capitalized by several neurotrasmitter reuptake systems, notably that concerning the synaptically-released glutamate removal by astrocytes, without apparent ATP hydrolysis. Thus, since these mechanisms can be rephrased in terms of $\text{Na}^+/\text{K}^+-\text{ATPase}$ activity, it has been argued that from an energetic point of view it is conceivable to take into account the sole

Table 3: Values of model parameters.

Parameter	Value	Parameter	Value
S_m/V_{n}	9×10^4 cm^{-1}	K_{eG}	10 mmol/L
S_m/V_{g}	3.5×10^4 cm^{-1}	$R_{\mathrm{eG,oo}}$	1.0
$g_{\mathrm{Na}}^{\mathrm{x}}$	0.0039 mS/cm^2	$R_{\mathrm{eG,oi}}$	1.0
V_m^{n}	-70 mV	$R_{\mathrm{eG,io}}$	1.0
V_m^{g}	-80 mV	$R_{\mathrm{eG,ee}}$	1.0
k_{Pump}	0.29×10^{-6} cm/mmol/L/s	K_{gG}	10 mmol/L
$K_{m,\mathrm{Pump}}$	0.5 mmol/L	$R_{\mathrm{bgG,oo}}$	1.0
v_1^{n}	0.39-0.41 mmol/L/s	$R_{\mathrm{bgG,oi}}$	1.0
v_2^{n}	18.0-18.4 mmol/L/s	$R_{\mathrm{bgG,io}}$	0.76
v_1^{g}	0.12-0.21 mmol/L/s	$R_{\mathrm{bgG,ee}}$	0.76
v_2^{g}	11.7-19.7 mmol/L/s	$R_{\mathrm{giG,oo}}$	1.0
$\tau_{\mathrm{Stim}}^{\mathrm{x}}$	2 s	$R_{\mathrm{giG,oi}}$	1.0
$k_{\mathrm{HKPFK}}^{\mathrm{n}}$	0.11 s^{-1}	$R_{\mathrm{giG,io}}$	1.36
$k_{\mathrm{HKPFK}}^{\mathrm{g}}$	0.06 s^{-1}	$R_{\mathrm{giG,ee}}$	1.36
$K_{I,\mathrm{ATP}}$	1 mmol/L	K_{nG}	4 mmol/L
nH	4	$R_{\mathrm{nG,oo}}$	1.0
K_g	0.05 mmol/L	$R_{\mathrm{nG,oi}}$	1.0
$k_{\mathrm{PGK}}^{\prime \mathrm{m}}$	42.6 L/mmol/s	$R_{\mathrm{nG,io}}$	0.72
$k_{\mathrm{PGK}}^{\prime \mathrm{g}}$	23.6 L/mmol/s	$R_{\mathrm{nG,ee}}$	0.72
$k_{\mathrm{PK}}^{\mathrm{n}}$	86.7 L/mmol/s	K_{eL}	1×10^{-4} mmol/L
$k_{\mathrm{PK}}^{\mathrm{g}}$	48.2 L/mmol/s	$R_{\mathrm{eL,oo}}$	1.0
$k_{\mathrm{LDH}}^{\mathrm{n}+}$	2000 L/mmol/s	$R_{\mathrm{eL,oi}}$	1.0
$k_{\mathrm{LDH}}^{\mathrm{n}-}$	44.8 L/mmol/s	$R_{\mathrm{eL,io}}$	0.71
$k_{\mathrm{LDH}}^{\mathrm{g}+}$	1111 L/mmol/s	$R_{\mathrm{eL,ee}}$	0.71
$k_{\mathrm{LDH}}^{\mathrm{g}-}$	24.9 L/mmol/s	K_{gL}	2×10^{-4} mmol/L
$V_{max,\mathrm{Mito}}^{\mathrm{n}}$	0.0185 mmol/L/s	$R_{\mathrm{bgL,oo}}$	1.0
$V_{max,\mathrm{Mito}}^{\mathrm{g}}$	0.0102 mmol/L/s	$R_{\mathrm{bgL,oi}}$	0.54
$K_{m,\mathrm{Mito}}$	0.05 mmol/L	$R_{\mathrm{bgL,io}}$	0.54
$K_{m,\mathrm{O2}}$	0.001 mmol/L	$R_{\mathrm{bgL,ee}}$	0.08
$K_{m,\mathrm{ADP}}^{x}$	0.005 mmol/L	$R_{\mathrm{giL,oo}}$	1.0
$k_{\mathrm{CK}}^{\mathrm{n}+}$	0.37 L/mmol/s	$R_{\mathrm{giL,oi}}$	0.54
$k_{\mathrm{CK}}^{\mathrm{n}-}$	0.002 L/mmol/s	$R_{\mathrm{giL,io}}$	0.54
$k_{\mathrm{CK}}^{\mathrm{g}+}$	0.204 L/mmol/s	$R_{\mathrm{giL,ee}}$	0.08
$k_{\mathrm{CK}}^{\mathrm{g}-}$	0.0011 L/mmol/s	K_{nL}	2×10^{-5} mmol/L
$PS_{\mathrm{c}}/V_{\mathrm{n}}$	1.58 s^{-1}	$R_{\mathrm{nL,oo}}$	1.0
$PS_{\mathrm{c}}/V_{\mathrm{g}}$	0.83 s^{-1}	$R_{\mathrm{nL,oi}}$	2.0
K_{O2}	0.0361 mmol/L	$R_{\mathrm{nL,io}}$	2.0
[Hb]OP_{Hb}	8.6 mmol/L	$R_{\mathrm{nL,ee}}$	3.0
nh	2.73	$T_{max,\mathrm{GLC}}^{\mathrm{ce}}$	5.692 mmol/L/s
[O$_{2\mathrm{a}}$]	8.34 mmol/L	$T_{max,\mathrm{LAC}}^{\mathrm{ce}}$	0.264 mmol/L/s
[GLC$_{\mathrm{a}}$]	6 mmol/L	$T_{max,\mathrm{GLC}}^{\mathrm{eb}}$	6.408 mmol/L/s
[LAC$_{\mathrm{a}}$]	1 mmol/L	$T_{max,\mathrm{LAC}}^{\mathrm{eb}}$	0.297 mmol/L/s
α_F	0.7	$T_{max,\mathrm{GLC}}^{\mathrm{bg}}$	0.07 mmol/L/s
CBF_0	0.012 s^{-1}	$T_{max,\mathrm{LAC}}^{\mathrm{bg}}$	0.029 mmol/L/s
t_1	5 s	$T_{max,\mathrm{GLC}}^{\mathrm{gi}}$	0.025 mmol/L/s
A	2.212 mmol/L	$T_{max,\mathrm{LAC}}^{\mathrm{gi}}$	0.585 mmol/L/s
C	10 mmol/L	$T_{max,\mathrm{GLC}}^{\mathrm{in}}$	0.581 mmol/L/s
N	0.212 mmol/L	$T_{max,\mathrm{LAC}}^{\mathrm{in}}$	0.256 mmol/L/s
[Na$_{\mathrm{i}}^{+}$]	150 mmol/L	$k_{Diff,\mathrm{GLC}}^{\mathrm{bi}}$	0.023 s^{-1}
[H^{+}]	62.5 nmol/L	$k_{Diff,\mathrm{LAC}}^{\mathrm{bi}}$	0.023 s^{-1}

Parameter correspond to published *in vivo* experimental data when possible, otherwise they were calculated in order to find experimental stationary metabolites concentrations.

Na$^+$ dynamics [93, 118]. In the steady-state, this notion is granted by the fact that both Na$^+$ and K$^+$ must separately have their ohmic leakage exactly matched by their active pumping rates. Moreover, preserving ion homeostasis requires the validity of this simplified proposition with respect to activation-related phenomena.

The leakage Na$^+$ current is mathematically described by the Hodgkin-Horowicz formula, which is given by

$$J_{\text{Na}^+}^{Leak} = \frac{S}{V}\frac{g_{\text{Na}^+}}{F}\left(E_{\text{Na}^+} - V_m\right) = \frac{S}{V}\frac{g_{\text{Na}^+}}{F}\left(\frac{RT}{F}\ln\frac{[\text{Na}^+]_\text{o}}{[\text{Na}^+]_\text{i}} - V_m\right) \tag{15}$$

where E_{Na^+} is the Nernst potential for sodium and V_m is the membrane potential. Both the membrane potential V_m and the extracellular sodium concentration $[\text{Na}^+]_\text{o}$ are assumed as constants (see [118]). In equation (15) F is the Faraday constant, R the gas constant, T the absolute temperature, S the cell surface area, V the intracellular volume, and g_{Na^+} the sodium conductance of the membrane. Sodium leakage determines the resting ATP hydrolysis by the Na$^+$/K$^+$–ATPase. Considering the biophysical properties of human cortical cellular membranes and assuming that the ATP consumption equals one third of the sodium load into cells, it has been calculated that the energy needed for Na$^+$ extrusion pertaining to resting membrane potentials is about 3-fold greater in neurons than in astrocytes [93, 94].

A.3 Na$^+$/K$^+$–ATPase

At rest, energy is required by the Na$^+$/K$^+$–ATPase for the maintenance of resting membrane potentials. During brain activation sodium flux into cells is enhanced, which further activates the pump and augment the demand for ATP. To a first approximation, the velocity of the pump is supposed to depend on ATP concentration via standard Michaelis-Menten kinetics and intracellular Na$^+$ [14] according to the formula

$$v_{\text{Pump}} = \frac{S}{V}k_{\text{Pump}}[\text{ATP}][\text{Na}^+]_\text{i}\left(1 + \frac{[\text{ATP}]}{K_{m,\text{Pump}}}\right)^{-1} \tag{16}$$

where k_{Pump} is the rate constant of the pump, $K_{m,\text{Pump}}$ the Michaelis-Menten constant for ATP, and $[\text{ATP}]$ and $[\text{Na}^+]_\text{i}$ the intracellular ATP and sodium concentration, respectively.

A.4 Stimulation-derived Na$^+$ influx

The Na$^+$ entry into individual neurons and astrocytes due to their electrical activity in terms of ionic channels or neurotransmitter receptors is described globally because of channels distribution differences among brain cells, and the lack of models about several physiologic mechanisms such as habituation. Modeling evidence has been produced that the inward flow of Na$^+$ ions into cells cannot be restricted to action potentials, because only neuronal axons and somata are concerned [118]. More physiological results have been obtained considering the involvement of synaptic potentials [10], whose theoretical account is based on the time-course of intracortical electrophysiologic recordings [91]. Accordingly, synaptic activity (which encompasses neuronal habituation processes) results in a varying velocity—i.e. a decay—of sodium inrush into neurons and astrocytes. Thus, during a sustained activation (for $0 \le t \le t_{end}$) it is convenient to assume a time-dependent sodium flow of the form

$$J_{\text{Na}^+}^{\text{Stim}} = v_1 + v_2\frac{t}{\tau}\exp\left(-\frac{t}{\tau}\right) \tag{17}$$

that is a constant term plus an alpha function, where v_1, v_2 and τ parameters depend on the cell type and on the chosen stimulation paradigm [10, 11]. It should be realized that a theoretical characterization of Na$^+$ influx into astrocytes due to glutamate uptake is currently unfeasible, nor it is the knowledge of a putative differential representation between the explicit neuronal and astrocytic time-dependent stimulation term. However, since the different time scale between Na$^+$ movements across cells (milliseconds) and changes in metabolites concentration (seconds), the exact time-course of sodium entrance into cells is thought to be not critical [10, 11]. Nonetheless, it was the alteration of the relative neuronal versus astrocytic stimulation magnitude to conducts the model outcomes toward diverging interpretations [11].

A.5 Adenosine triphosphate homeostasis

The production of adenosine triphosphate in the brain is regulated in order to maintain a high and far from equilibrium ATP concentration. Although its terminal phosphate groups have a very rapid turnover [120], ATP is kept at relatively constant level by an efficient control of ADP phosphorylation with respect to ATP hydrolysis, resulting in a stable net sum of fast synthesis and utilization. Cerebral cells are thought to have both high and fluctuating energy requirements, which can seldom be met by glucose catabolism alone via glycolysis and oxidative phosphorylation [121]. On the basis of the current evidence, it appears that two much faster mechanisms have evolved that act in concert to reduce the potential limitations for energy usage by ATPases which may be induced by the localized pile up of ATP or ADP [65]. These energy buffer systems are based on the reversible transfer of phosphate groups by protein kinases, thereby facilitating all those processes that would otherwise depend entirely on the free diffusion of ATP and ADP. The importance of the implicated enzymes—i.e. adenylate kinase and creatine kinase—in the brain indicates that diffusion alone is insufficient to sustain the physiologic energetic provisions to neural cells [117].

Accumulation of ADP derived from increased energy demand is prevented by the active adenylate kinase (AK) reaction, which forms equivalent amounts of ATP and AMP from ADP. The enzymatic activity of AK provides a sensitive control for the maintenance of cellular ATP concentration, because a rise in AMP level

trigger the activation of AMP kinase, which in turn is a positive modulator of ATP synthesis [122]. The transport of ATP equivalents between sites of production and sites of consumption is significantly reinforced by the creatine-phosphocreatine shuttle, which relies on the enzyme creatine kinase (CK) catalyzing the transfer of phosphate groups from phosphocreatine (PCr) to creatine (Cr).

A.6 Adenylate kinase

In the brain, the adenylate kinase (AK)-catalyzed reaction is close to equilibrium [49], with an equilibrium constant given by

$$q_{\text{AK}} = \frac{[\text{ADP}]^2}{[\text{AMP}][\text{ATP}]} \tag{18}$$

Considering the conserved moiety of adenosine nucleotides, namely

$$A = [\text{AMP}] + [\text{ADP}] + [\text{ATP}] \tag{19}$$

this allows to express ADP and AMP concentration as a function of ATP concentration, total adenylates and equilibrium constant q_{AK} [123]. In particular, ADP concentration is written by

$$[\text{ADP}] = \frac{[\text{ATP}]}{2} \left[-q_{\text{AK}} + \sqrt{q_{\text{AK}}^2 + 4q_{\text{AK}} \left(\frac{A}{[\text{ATP}]} - 1 \right)} \right] \tag{20}$$

This leads to the equation

$$\frac{d[\text{AMP}]}{d[\text{ATP}]} = -1 + \frac{q_{\text{AK}}}{2} - \frac{1}{2} \sqrt{q_{\text{AK}}^2 + 4q_{\text{AK}} \left(\frac{A}{[\text{ATP}]} - 1 \right)} +$$
$$+ \frac{q_{\text{AK}} A}{[\text{ATP}]\sqrt{q_{\text{AK}}^2 + 4q_{\text{AK}} \left(\frac{A}{[\text{ATP}]} - 1 \right)}} \tag{21}$$

which results in the possibility to neglect the explicit reaction expression and include the effect of AK in the derivative of ATP concentration [14].

A.7 Creatine kinase

The velocity of the creatine kinase (CK)-catalyzed reaction can be calculated according to several models [124–126]. However, the effect of phosphocreatine (PCr) and creatine (Cr) in buffering ATP level can be simplified by reducing the CK system to a single reaction [118]. Accordingly, it is possible to formulate the reversible reaction velocity as

$$v_{\text{CK}} = k_{\text{CK}}^+ [\text{PCr}][\text{ADP}] - k_{\text{CK}}^- [\text{Cr}][\text{ATP}] \tag{22}$$

where k_{CK}^+ and k_{CK}^- are the second-order rate constants for the direct and inverse reaction, respectively. The total creatine level is written as

$$C = [\text{PCr}] + [\text{Cr}] \tag{23}$$

and it is held constant. Given ample cerebral phosphocreatine, the creatine-phosphocreatine shuttle system can generate ATP at a rate that is ten times faster than oxidative phosphorylation and 40 times faster than glycolysis [121]. Recently, putative neuron-glia relationships have been suggested with respect to the phosphocreatine shuttle [127], which could reflect the distinct cellular expression of CK isoenzymes and creatine transporters [128]. However, the significance of intercellular creatine exchanges in the physiologic brain energy homeostasis is presently not established.

A.8 Glycolysis

The first step in the catabolism of glucose molecule is glycolysis (also known as the Embden-Meyerhoff pathway), which results in the net production of 2 molecules of ATP per glucose, following the attachment of another phosphate to ADP by means of cytoplasmic substrate-level phosphorylation. Besides the importance of glycolytic metabolism in regulating the cellular energy production due to its sensitivity to ATP concentration [120, 129], it plays a major role in brain energetics since it determines the rate of intracellular glucose catabolism, and hence its cerebral metabolic rate (CMRGlc). Validated theoretical descriptions of the glycolytic pathway have been achieved based on a simplified model of erythrocyte glycolysis, embracing the explicit description of the sole reactions catalyzed by regulatory enzymes, namely hexokinase (HK), phosphofructokinase (PFK), phosphoglycerate kinase (PGK), and pyruvate kinase (PK) [14, 130, 131].

The activity of hexokinase (HK) and phosphofructokinase (PFK) is lumped together in a single term, which takes into account the inhibition by ATP following Hill equation [14] and the glucose tissue concentration via Michaelis-Menten kinetics [49], thus obtaining a velocity for the HK-PFK system given by

$$v_{\text{HK}-\text{PFK}} = k_{\text{HK}-\text{PFK}}[\text{ATP}] \left[1 + \left(\frac{[\text{ATP}]}{K_{I,\text{ATP}}} \right)^n \right]^{-1} \left(1 + \frac{K_g}{[\text{GLC}]} \right)^{-1} \tag{24}$$

where $k_{\mathrm{HK-PFK}}$ is the first-order rate constant, $K_{I,\mathrm{ATP}}$ is the inhibition constant for ATP with n as its Hill coefficient, and K_g is the Michaelis-Menten constant for glucose. The velocity of phosphoglycerate kinase (PGK) can be written as

$$v_{\mathrm{PGK}} = k_{\mathrm{PGK}}[1,3\mathrm{BPG}][\mathrm{ADP}] \tag{25}$$

where $[1,3\mathrm{BPG}]$ is the 1,3-bisphosphoglycerate concentration, and k_{PGK} is the second-order rate constant in which it is assumed that the enzyme velocity is proportional to the product of concentrations of its substrates [14]. However, it is possible to not consider explicitly the 1,3BPG concentration by taking into account that the glyceraldehyde-phosphate dehydrogenase (GAPDH)-catalyzed reaction is almost at equilibrium, which leads to an equilibrium constant given by

$$q_{\mathrm{GAPDH}} = \frac{[1,3\mathrm{BPG}][\mathrm{NADH}]}{[\mathrm{GAP}][\mathrm{NAD^+}][\mathrm{P_i}]} \tag{26}$$

where $[\mathrm{GAP}]$ is the glyceraldehyde-phosphate concentration and $[\mathrm{NAD^+}]$ and $[\mathrm{NADH}]$ are the nicotinamide adenine dinucleotide and its reduced counterpart, respectively, whose total concentration

$$N = [\mathrm{NADH}] + [\mathrm{NAD^+}] \tag{27}$$

is constant. Since the concentration of inorganic phosphate $[\mathrm{P_i}]$ is supposed to vary slightly [14,118], equation (25) can be written as

$$v_{\mathrm{PGK}} = k'_{\mathrm{PGK}}[\mathrm{GAP}][\mathrm{ADP}]\frac{[\mathrm{NAD^+}]}{[\mathrm{NADH}]} \tag{28}$$

where the term $k'_{\mathrm{PGK}} = k_{\mathrm{PGK}} q_{\mathrm{PGKDH}}[\mathrm{P_i}]$ is constant. The reaction catalyzed by pyruvate kinase (PK) obeys second-order kinetics [14], and can be written as

$$v_{\mathrm{PK}} = k_{\mathrm{PK}}[\mathrm{PEP}][\mathrm{ADP}] \tag{29}$$

where k_{PK} is the relative rate constant, and $[\mathrm{PEP}]$ the phosphoenolpyruvate concentration. The reversible conversion of pyruvate to lactate is accomplished by lactate dehydrogenase (LDH), whose reaction velocity is given by

$$v_{\mathrm{LDH}} = k^+_{\mathrm{LDH}}[\mathrm{PYR}][\mathrm{NADH}] - k^-_{\mathrm{LDH}}[\mathrm{LAC}][\mathrm{NAD^+}] \tag{30}$$

where k^+_{LDH} and k^-_{LDH} are the second-order rate constants for the direct and inverse reaction, respectively [118].

Under both aerobic and anaerobic conditions, considerable lactate is produced in the brain by glycolysis. Conversion of lactate to pyruvate by LDH is thus necessary for further metabolism of lactate through the tricarboxylic acid cycle (see below). The enzyme LDH exists in five isoforms (LDH1–5), consisting of tetramers formed from two distinct subunits (M and H) and exhibiting slightly different kinetic properties with respect to rates of catalysis and affinities for pyruvate. Moreover, there is a differential enrichment of LDH M4 and M3H isoforms in astrocytes and H4 and H3M in neurons [132]. It must be realized, however, that LDH isoforms predominance within a cellular compartment cannot control *per se* the direction of lactate dehydrogenation [117].

A.9 Mitochondrial respiration

In order for glucose to be completely oxidized to CO_2, pyruvate formed in glycolysis (or derived from lactate dehydrogenation) is converted to acetyl coenzyme A (acetyl-CoA) by the multienzyme complex of pyruvate dehydrogenase (PDH), which is localized in mitochondria. The PDH complex controls the rate of pyruvate entry in the tricarboxylic acid (TCA) cycle and the subsequent oxygen-dependent mitochondrial respiration by becoming more active under states of greater metabolic activity, which is distinguished for increased pyruvate and ADP concentrations and decreased acetyl-CoA and ATP levels [117].

When the rate of pyruvate production through glycolysis exceeds pyruvate utilization by TCA cycle, the end-product of glycolysis is lactate, albeit in the brain considerable lactate is produced under both aerobic and anaerobic conditions. Conversion of pyruvate to lactate is carried out by lactate dehydrogenase (LDH), and allows the regeneration of NAD^+ which is essential to maintain a continued glycolytic flux. Furthermore, pyruvate dehydrogenation by PDH is inhibited by NADH, thereby reducing the formation of acetyl-CoA by pyruvate allowing more pyruvate to be reduced to lactate in order to restore the NAD^+ necessary to sustain glycolysis [98]. The condition of enhanced lactate production has been well described in skeletal muscle during intense exercise and appears to share similarities with the transient uncoupling between glucose and oxygen consumptions observed in stimulated human cerebral cortex [5]. Although the oxidation of pyruvate is subject to control at several enzymatic steps, it has been put forward that a simplified description based essentially on substrates availability—i.e. pyruvate, oxygen and ADP—can be adopted [10,49,133].

The various aspects of mitochondrial respiration, which include shuttle systems for reducing equivalents, tricarboxylic-acid cycle and oxidative phosphorylation can be thus grouped together in a single term v_{Mito}, which is assumed to be equal to the velocity of pyruvate dehydrogenase [10,11]. Accordingly, v_{Mito} depends on intracellular pyruvate, oxygen and ADP concentration conforming to the Michaelis-Menten kinetics [49,133], which can be written as

$$v_{\mathrm{Mito}} = V_{max,\mathrm{Mito}}\left(1 + \frac{K_{m,\mathrm{Mito}}}{[\mathrm{PYR}]}\right)^{-1}\left(1 + \frac{K_{\mathrm{O2}}}{[\mathrm{O_2}]}\right)^{-1}\left(1 + \frac{K_{m,\mathrm{ADP}}}{[\mathrm{ADP}]}\right)^{-1} \tag{31}$$

where $V_{max,\mathrm{Mito}}$ is the maximum velocity of the mitochondrial respiration, and $K_{m,\mathrm{Mito}}$, K_{O2}, and $K_{m,\mathrm{ADP}}$ are the Michaelis-Menten constants for pyruvate, oxygen and ADP, respectively.

A.10   Nutrients transport

The amount of energy available limits the capacity of the brain to effectively process information [20]. Accordingly, blood flow is increased to brain areas where nerve cells are active, in an independent fashion with respect to the global brain perfusion [134]. Cerebral blood flow (CBF) is controlled by smooth muscle cells surrounding precapillary arterioles, which are thought to constrict or dilate in response to the activity of dedicated neuronal networks, thus providing a coupling mechanism between activity and blood flow control. However, currently there is not a complete understanding of the fundamental mechanisms responsible for the regulation of local CBF, where a variety of factors are likely to contribute [2].

Regardless of the exact physiologic determinant, there is a rise in the local CBF in order to adapt the nutrients delivery to the increased metabolic needs after brain activation. Under normal conditions, CBF is readily raised to a new stationary level for the entire duration of the stimulus [135], thereby determining an increase in the fraction of extraction and wash out of nutrient molecules such as glucose, oxygen and lactate [10].

The increase in cerebral blood flow (CBF) accounts for substrates supply and/or clearance through the blood-brain barrier (BBB). It can be modeled as a trapezoidal function [135] given by

$$\text{CBF}(t) = \begin{cases} (1 + \alpha_F)\text{CBF}_0 & t_1 \leq t \leq t_{end} \\ \text{CBF}_0 & t < 0, t > t_{end} + t_2 \end{cases} \tag{32}$$

where CBF_0 is the blood flow value at rest, α_F is the CBF increase fraction, t_{end} is the duration of the stimulation, and t_1 and t_2 are the durations of the up and down ramps so that CBF(t) increases and decreases linearly for $0 \leq t \leq t_1$ and $t_{end} \leq t \leq t_{end} + t_2$, respectively. For $t_1 = t_2$ the function CBF(t) described by equation (32) is symmetrical [10]. The CBF regulates the capillary glucose ($[\text{GLC}]_{\text{cap}}$), lactate ($[\text{LAC}]_{\text{cap}}$) and oxygen ($[\text{O}_2]_{\text{cap}}$) concentration following mass balance [118], which results in flow equations given by

$$j^c_{\text{GLC}} = 2\text{CBF}(t)\left([\text{GLC}]_{\text{serum}} - [\text{GLC}]_{\text{cap}}\right) \tag{33}$$

$$j^c_{\text{LAC}} = 2\text{CBF}(t)\left([\text{LAC}]_{\text{serum}} - [\text{LAC}]_{\text{cap}}\right) \tag{34}$$

$$j^c_{\text{O}_2} = 2\text{CBF}(t)\left([\text{O}_2]_{\text{serum}} - [\text{O}_2]_{\text{cap}}\right) \tag{35}$$

where $[\text{GLC}]_{\text{serum}}$, $[\text{LAC}]_{\text{serum}}$ and $[\text{O}_2]_{\text{serum}}$ are the glucose, lactate and oxygen serum concentrations, respectively.

The delivery of nutrients to brain cells and the their intercellular trafficking is modulated by a number of transporters existing in several isoforms. In particular, the facilitated transport of both glucose and lactate is mediated by a specific family of transporter proteins (GLUTs and MCTs, respectively), whose members have distinct cellular expression patterns and different kinetic properties [12]. Traditionally, carrier-mediated nutrients transport to the brain has been indeed described by standard symmetric Michaelis-Menten kinetics, with the reversible model being more appropriate than the unidirectional product formation model [10, 136]. However, a more adequate description takes into account the asymmetric transport kinetic properties as accounted for by the distinct modes of transport of these carriers, namely equilibrium exchange, zero-trans entry, and zero-trans exit [12]. Mathematically this reduces to a single equation, which is given by

$$J_G = T_{\text{G},max} \frac{[\text{G}]_{\text{o}}\left(K + [\text{G}]_{\text{i}}\right) - [\text{G}]_{\text{i}}\left(K + [\text{G}]_{\text{o}}\right)}{K^2 + KR_{\text{io}}[\text{G}]_{\text{o}} + KR_{\text{oi}}[\text{G}]_{\text{i}} + R_{\text{ee}}[\text{G}]_{\text{o}}[\text{G}]_{\text{i}}} \tag{36}$$

where $T_{\text{G},max}$ is the maximum transport rate, K is an affinity term and R_{ee}, R_{oi} and R_{io} are the resistance terms for equilibrium exchange, zero-trans entry, and zero-trans exit, respectively [12]. In equation (36) G is the involved substance and o and i subscripts refer to either extra- or intracellular compartment, respectively. It is worth mentioning that the transport of nutrients in the brain may change under certain conditions by means of upregulation or downregulation of transporter proteins at the cerebral endothelium [137]. However, it is not known whether the adaptation of the properties of these transporters due to alteration of protein expression is significantly involved under physiological levels of brain activation [138].

Brain homeostasis is controlled by the blood-brain barrier (BBB), an active membrane system which maintains an appropriate cellular environment by limiting the transport of substances to the tissue via both physical and metabolic barriers. In particular, the lumen of cerebral capillaries is completely encircled by endothelial cells, which form cell-to-cell seal tight junctions resulting in a very low paracellular permeability. Interestingly, numerous structural, pharmacological and biochemical studies have found a polarization of receptors, enzymes and channels at the cerebral endothelia (see [139]).

Transit across the BBB involves translocation through lumenal membrane, internal cytoplasmic domain, and ablumenal membrane of the capillary endothelium. Moreover, the ablumenal surface of the endothelium is supported by a thin basement membrane—i.e. basal lamina—consisting of proteins belonging to the extracellular matrix (ECM). The basal lamina, which is shared by endothelial cells as well as by pericytes and astrocytic endfeet providing mechanical support for cell attachment, can act as a barrier to the passage of macromolecules. Microvascular pericytes send out cellular projections covering approximately 20-30% of the vascular circumference [140]. Astrocytes, on the contrary, envelop more than 99% of the BBB endothelium, resulting in a ~ 20 nm gap between adjacent astrocytes [12]. Nevertheless, this separation is readily diffusible by horseradish peroxidase (HRP) as demonstrated by intracerebroventricular injection into the cerebrospinal fluid [141]. Since HRP is considerably larger than brain metabolites such as glucose and lactate, it is likely that astrocytes do not contribute to the physical barrier of the BBB. Thus, because the layer of astrocytic endfeet surrounding blood capillaries does not constitute a impediment to permeation of basal lamina, free molecular diffusion may contribute significantly to the transport of nutrients into interstitium [12]. However, the degree of obstruction placed by dead-end spaces and the extensive mesh of intertwined fibrous proteins and proteoglycans of the ECM in the proximity of the sole basement membrane remains difficult to ascertain.

Howsoever, besides facilitative transport glucose and lactate entry/exit to/from the brain occurs also through diffusion across the endothelial cell layer. The free diffusion of a substance in the ECS can be described theoretically by the diffusion coefficient D as well as by the tortuosity factor λ, which represents the hindrance imposed on diffusing molecules by the tissue with respect to an obstacle-free medium [142]. These two values constitute the apparent diffusion coefficient (ADC), which equals D/λ. The apparent rate constant k_{app} for molecular diffusion between regions separated by a distance ϕ is thus given by

$$k_{\text{app}} = \frac{\text{ADC}}{\phi^2} = \frac{D}{\lambda\phi^2} \tag{37}$$

where ϕ can be taken as the average midpoint between adjacent brain capillaries [12].

A somewhat different treatment is needed for oxygen transport through the BBB, which operates by simple diffusion according to Fick's law [10, 49, 143]. The velocity of oxygen transport depends on the BBB surface S_{cap} and permeability P, as well as on the oxygen concentration gradient between blood and tissue, according to the equation

$$J_{\text{O2}} = \frac{PS_{\text{cap}}}{V_{\text{cap}}} \left([\text{O}_2]_{\text{plasma}} - [\text{O}_2]_{\text{tissue}}\right) \tag{38}$$

where V_{cap} is the capillary volume. It is generally assumed that the average concentration of oxygen inside the capillary $[\text{O}_2]_{\text{cap}}$ is related to the average plasma oxygen concentration $[\text{O}_2]_{\text{plasma}}$ via the classical Hill equation [49, 143], which can be written as

$$[\text{O}_2]_{\text{cap}} = [\text{Hb}]OP_{\text{Hb}} \left[1 + \left(\frac{K_{\text{O2}}}{[\text{O}_2]_{\text{plasma}}}\right)^n\right]^{-1} \tag{39}$$

where n is the Hill coefficient, $[\text{Hb}]$ is the hemoglobin concentration, OP_{Hb} is hemoglobin oxiphoric power—i.e. the maximum number of O_2 molecules carried by one molecule of hemoglobin—and K_{O2} is the product of oxygen p_{50} by the O_2 solubility coefficient. Inverting (39) for $[\text{O}_2]_{\text{plasma}}$ and inserting it into (38) gives

$$J_{\text{O2}} = \frac{PS_{\text{cap}}}{V_{\text{cap}}} \left[\frac{K_{\text{O2}}}{\left(\frac{[\text{Hb}]OP_{\text{Hb}}}{[\text{O}_2]_{\text{cap}}} - 1\right)^{1/n}} - [\text{O}_2]_{\text{tissue}}\right] \tag{40}$$

which relates the blood-tissue flux of oxygen to the relevant concentrations.